Chapter 2

Internal Friction in Magnesium Alloys and Magnesium Alloys-Based Composites

Zuzanka Trojanová, Peter Palček, Pavel Lukáč and

Mária Chalupová

Additional information is available at the end of the chapter

http://dx.doi.org/10.5772/67028

Abstract

In practice, some problems connected with undesirable mechanical vibrations or interruption of acoustic bridges may be solved using high damping materials. Especially, transport industry needs high damping light materials with proper mechanical properties. Magnesium alloys and magnesium alloys-based metal matrix composites may be considered as materials exhibiting such behaviour. Damping of mechanical vibrations and their conversion to the heat (internal friction) is conditioned by the movement and redistribution of various defects in the crystal lattice. Generally, internal friction depends on the material microstructure and conversely changes in the material microstructure may be studied using the internal friction measurements. The strain amplitude-dependent internal friction was investigated at room temperature in commercially available Mg alloys and Mg alloys-based composites with the aim to identify changes in the microstructure invoked by thermal and mechanical loading. The temperature-dependent internal friction indicated the following effects: (a) mechanisms connected with dislocations and grain boundaries in the microcrystalline pure Mg, (b) precipitation and phase transformations in alloys and (c) generation as well as relaxations of thermal stresses in composites. The internal friction was measured in the bending mode in two frequency regions: I.: units and tens of Hz and II.: units of kHz.

Keywords: magnesium alloys, magnesium alloys-based composites, amplitude-dependent internal friction, temperature-dependent internal friction, dislocations, solute atoms, thermal stresses

1. Introduction

Internal friction is an anelastic relaxation connected with dissipation of the mechanical energy carried by the sonic or ultrasonic wave in a material and their conversion mostly into heat. In a solid material, it is manifested by deviations from Hooke's law and stress-strain hysteresis in the case of cyclic loading. Defects in the microstructure as point defects, grain boundaries, phase transformations, electrons, phonons or redistribution of the heat are responsible for internal friction. The general quantities describing the internal friction is the *specific damping capacity* $\Psi = \Delta W_{diss}/W_{max}$, or the *loss factor* $\eta = \Delta W_{diss}/2\pi W_{max}$, where ΔW_{diss} is the mechanical energy dissipated in a material during one cycle of the applied stress, and W_{max} is the maximum mechanical energy stored in it. In real experiments depending on the apparatus used, various quantities are measured: the mechanical loss factor tanφ, the logarithmic decrement δ or the reciprocal value of the quality factor Q. These quantities are simply proportional:

$$\Psi = \eta/2\pi = \tan\varphi = \delta/\pi = Q^{-1}. \tag{1}$$

It should be mentioned that such proportionality is valid for small values of damping $\Psi<<1$, which is valid for most metallic materials. Very effective sources of internal friction are dislocations. If a material containing dislocations is submitted to a harmonic applied stress $\sigma = \sigma_0 \sin\omega t$ with an angular frequency $\omega = 2\pi f$, the lost energy ΔW_{diss} depends only on the anelastic strain. In the case of an anelastic dislocation strain

$$\Delta W_{diss} = \oint \varepsilon_d \, d\sigma. \tag{2}$$

The maximum stored energy can be well approximated by the maximum elastic stored energy

$$W_{max} = \int_0^{\sigma_0} \sigma d\, \varepsilon_{el} = \frac{1}{2} J_{el} \sigma_0^2, \tag{3}$$

where J_{el} is the elastic compliance related to the shear modulus $G^{-1}=J_{el}$. Mechanical loss factor due to the presence of dislocations in the material may be written as

$$\tan\varphi = \frac{1}{\pi J_{el} \sigma_0^2} \oint \varepsilon_d \, d\sigma. \tag{4}$$

The logarithmic decrement, δ, as another damping quantity, is given as

$$\delta = \frac{1}{n} \ln \frac{A_i}{A_{i+n}}, \tag{5}$$

where A_i and A_{i+n} are the amplitudes of the ith cycle and $(i + n)$th cycle, respectively, separated by n periods of the free vibrations of the specimen.

In experiments, three types of dependences can be estimated:

(i) Amplitude (strain/stress) dependence of damping capacity;

(ii) Temperature dependence of the damping capacity;

(iii) Frequency dependence of the damping capacity.

Because the damping capacity is in many cases connected with the atomic jumps, Arrhenius equation may be used

$$f = f_0 \exp\left(-\Delta G/kT\right), \tag{6}$$

where f is frequency, f_0 a constant, ΔG the Gibbs free energy, k the Boltzmann constant and T the absolute temperature. In this way, the frequency dependence of the damping capacity may be converted to the temperature dependence.

The dynamic strain dependence of the damping capacity can be divided into a strain-independent and a strain-dependent component. If the logarithmic decrement is measured, the experimental finding can be expressed as

$$\delta = \delta_0 + \delta_H(\varepsilon), \tag{7}$$

δ_0 is the amplitude-independent component, found at low amplitudes. The component δ_H depends on the strain amplitude and it is usually caused by the presence of dislocations in the material. The strain amplitude dependence of the logarithmic decrement suggests dislocation-unpinning processes. Dislocations-solute atoms interactions may be explained using the Granato-Lücke (G-L) theory of dislocation internal friction. In the G-L theory [1, 2], the dislocation substructure exhibits longer segments with the lengths of L_N along which weak-pinning points (solute atoms) are randomly distributed. The mean distance between two weak-pinning points is ℓ assuming that $\ell \ll L_N$. The mean total density of dislocations is ρ. Shorter dislocation segments vibrate under the periodic stress $\sigma = \sigma_0 \sin\omega t$ carried with the sonic or ultrasonic wave. At $T = 0$ K and at sufficiently high stress, the dislocation is able to break away from the weak-pinning points which may be point defects (solute atoms) or their small clusters. The longer segments L_N are assumed to be determined by unbreakable pinning points, for example, the nodes of the Frank-Read sources. Dislocations break away from weak-pinning points under stress that is determined by the largest double loop in a segment. The length of this double loop is strongly dependent on the distribution of the solute atoms. The stress necessary for the break-away decreases with increasing temperature because the break-away process is thermally activated [3]. At higher temperatures, the break-away can

occur at lower stresses than necessary in pure mechanical process, but higher activation energies are required because the break-away is simultaneous from several neighbouring pinning points. In the high temperature and low frequencies approximation, the stress dependence of the decrement component δ_H can be expressed as [3]

$$\delta_H = \frac{\rho L_N^2}{6} \frac{\nu_d}{\omega} \left(\frac{3\pi kT}{2U_0}\right)^{1/2} \left(\frac{\ell^3 \sigma_0^2}{U_0 G}\right)^{1/2} \exp\left[-\frac{4}{3} \frac{U_0}{kT} \left(\frac{U_0 G}{\ell^3}\right)^{1/2} \frac{1}{\sigma_0}\right], \quad (8)$$

here G is the shear modulus, σ_0 is the amplitude of the applied stress and ω its angular frequency, ν is the dislocation frequency, U_0 is the activation energy, kT has its usual meaning. This relationship has a similar form as the original formula given by Granato and Lücke [1, 2]. The δ_H component depends exponentially on the stress amplitude. The amplitude-independent component δ_0 may be in the frame of G-L theory expressed as

$$\delta_0 = \frac{\Omega B \rho \ell^4 \omega}{E_L b^2}, \quad (9)$$

where Ω is an orientation factor, B is the coefficient of dislocation friction, E_L is the tension in a dislocation line and b is the Burgers vector of dislocations. The critical strain ε_{cr} at which the internal friction becomes amplitude dependent may be used to calculate the effective critical stress amplitude corresponding to the micro-yield stress according to the following equation:

$$\sigma_{cr} = E \varepsilon_{cr}, \quad (10)$$

where E is Young's modulus. The stress necessary for a thermal break-away of dislocation loops σ_T at a finite temperature is given by [3]

$$\sigma_T = \sigma_{cr} = \sigma_M \left[1 - \left(\frac{kT}{U_1} \ln A\right)^{2/3}\right] \quad (11)$$

with

$$A = \frac{2}{3} \frac{\nu}{\omega} \frac{\sigma_M}{\sigma_0} \left(\frac{kT}{U_1}\right)^{2/3}. \quad (12)$$

σ_M is assumed to be break-away stress in pure mechanical process. For a double loop with the loop length ℓ_1 and ℓ_2, it occurs at the stress

$$\sigma_M = \frac{2F_m}{b(\ell_1 + \ell_2)}. \quad (13)$$

Here, F_m is the maximum force between the dislocation and the pinning point. $U_1 = 4/3(F_m^3/\Phi)^{1/2}$, where Φ is a constant.

While amplitude-dependent component of internal friction is only due to the presence of dislocation in the material, amplitude-independent part is influenced by several contributions as dislocations, grain boundaries, precipitates, interfaces, or heat transfer. The damping capacity of materials is a function of the microstructure, stress, temperature, or frequency. The anelastic strain can result from the motion of structural defects, such as point defects, dislocation,

http://dx.doi.org/10.5772/67028

grain boundaries, and phase transformations, and conversely the internal friction can be used to study such motions. Two basic dependencies were measured: amplitude-dependent internal friction (ADIF) and temperature relaxation spectrum of internal friction (TDIF).

It is often stated in the literature that magnesium and magnesium alloys have good damping properties. Damping depends on many factors: purity, grain size, alloy composition, thermomechanical treatment of magnesium materials; their microstructure and substructure, temperature, frequency and the stress amplitude. Therefore the universal statement that magnesium and magnesium alloys have high damping capacity is not true. Experiments are necessary to establish to what extent damping occurs for each particular case. The first internal friction effect observed in magnesium was established by Kê [4]. One relaxation peak found at 490 K was attributed to the grain boundary sliding. Similar results of polycrystalline magnesium and magnesium alloys were found by several authors [5–11]. Internal friction peaks measured at low temperatures in magnesium by Fantozzi et al. [12] and Seyed Reihani et al. [13] were attributed to the so-called Bordoni relaxation, that is, the intrinsic mobility of dislocations through the Peierls barriers. Relaxation peaks found in the vicinity of 0.4 T_m observed by Nó et al. and Trojanová et al. were attributed to dislocation glide in the non-compact slip planes [14–16]. Ageing effects in magnesium alloys were studied using ADIF [17, 18] and also TDIF [19]. The influence of microplastic and cyclic deformation on the damping capacity was studied in Mg and Mg alloys using ADIF [8, 20, 21]. Formation of new interfaces in magnesium alloys via precipitation [22], mechanical twinning [23] or an adding of ceramic particles or fibres [24, 25] may substantially increase the damping capacity. Materials with the high damping capacity are known as HIDAMETS (HIgh DAmping MEtalS) or HIDAMATS (HIgh DAmping MAterialS) among them magnesium materials have an important place. Thermal cycling of magnesium alloys reinforced with ceramic fibres or particles may substantially deteriorate microstructure and mechanical properties [26].

2. Amplitude-dependent internal friction

2.1. Cast alloys

Gravity cast magnesium alloys AM20, AX41 and AZ31 were annealed step by step for 20 min at increasing temperature of the thermal cycle. The temperature step was 20°C. Immediately after thermal cycling, amplitude dependence of internal friction was measured. Amplitude dependences of decrement estimated for AM20 alloy are introduced in **Figure 1a–c** for various upper temperatures of the thermal cycle. The amplitude dependences of decrement are practically identical for thermal cycling with the upper temperatures up to 200 °C. Thermal cycling with higher temperatures between 200 and 260 °C causes a decrease in the amplitude dependent component while the amplitude independent component remains unchanged. Thermal cycling with the upper temperatures between 260 and 400 °C causes an increase in the amplitude dependent component. The amplitude dependence of decrement obtained at 400°C achieved similar values as in the case of the as-cast sample.

According to Eq. (8), the δ_H component of decrement depends exponentially on the stress amplitude. The experimental curves were fitted according to formula (8) in the form

$$\delta = \delta_0 + C_1 \varepsilon \exp(-C_2/\varepsilon), \quad (14)$$

Here, the C_1 parameter is proportional to $\ell^{2/3}$ and the C_2 is proportional to $\ell^{-2/3}$. Discussion of the C_2 parameter is simpler because it depends only on the length of the small dislocation segments ℓ and the activation energy U_0. Assuming that the activation energy is in the first approximation the same (all measurements were performed at room temperature), we may attribute observed temperature dependence of the C_2 parameter to changes in the microstructure. The typical feature of the microstructure of AM20 magnesium alloy is the formation of $Mg_{17}Al_{12}$ intermetallic phase particles as it is obvious from **Figure 2a**. The estimated parameters C_2 are shown in **Figure 1d**.

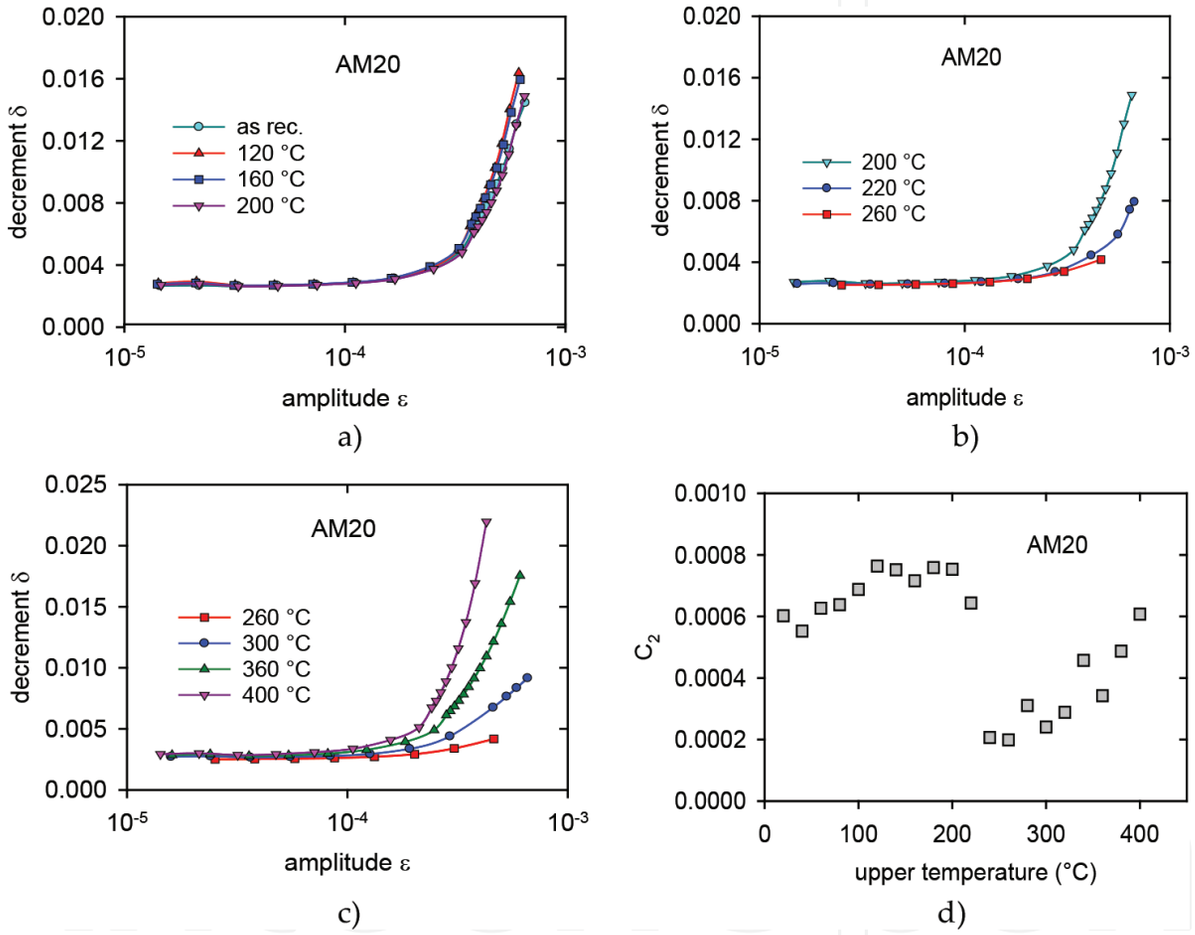

Figure 1. Amplitude dependence of decrement measured in the AM20 alloy after thermal cycling: lower (a), medium (b), higher (c) upper temperatures of the thermal cycle, temperature dependence of the C_2 parameter (d).

The temperature dependence of the C_2 parameter slightly increases up to 200°C, then rapidly decreases with increasing upper temperature of the thermal cycle, and starting from a temperature of 260-280°C, it again increases. The length of dislocation segments ℓ is done by the interaction of the solute atoms with the dislocation line. Although the concentration of solute atoms in the alloy is lower than the solubility limit, solute atoms in the as-cast alloy are not

http://dx.doi.org/10.5772/67028

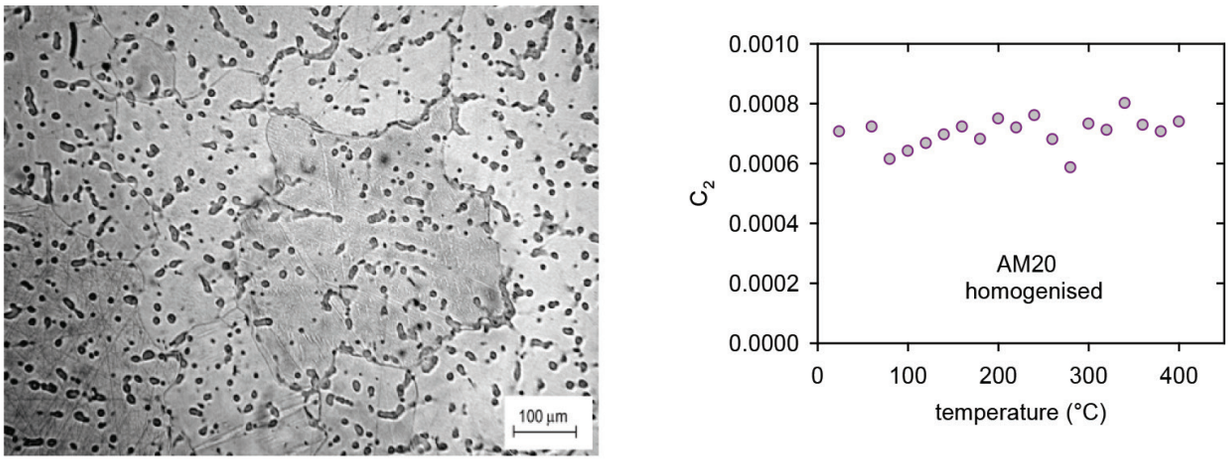

Figure 2. Microstructure of the as-cast alloy (a); temperature dependence of the C_2 parameter in the homogenised alloy alloy (homogenised is also in the picture above) alloy (b).

homogeneously dispersed. At temperatures between 200 and 320°C, solute atoms are movable and the solute solution is purified due to precipitation process in the alloy. Concentration of weak pinning points (solute atoms) decreases, and if the dislocation density is constant, the effective length ℓ of dislocation segments increases. The C_2 parameter is proportional to $C_2 \propto \ell^{-2/3}$, thus with increasing annealing temperature, the values of C_2 parameter decreases. Above 320°C, the C_2 slightly increases; this can be caused by several reasons: a decrease in dislocation density, ρ, thermal stresses and the interaction of dislocations with precipitates. The observed increase of C_2 parameter at temperatures up to 160°C could be caused by segregation of solute atoms at dislocations. Such processes were observed during plastic deformation of various Mg alloys [27, 28]. The strain-ageing phenomena are due to dislocation-solute atom interaction. After a homogenisation treatment (413°C for 18 h), free solute atoms occupy dislocation lines. In the G-L model, dislocations are pinned at some place and the free elastic segments move under the oscillating stress. Damping of these oscillations is controlled by interactions with phonons and electrons. In concentrated alloys, the dislocation line is strongly pinned by high number of solute atoms and their small clusters, which occupy the dislocation line. Because of very short distance between the weak pins (solute atoms), the force necessary for break-away of dislocation is very high. At $T = 0$, the dislocation starts to glide when the Peach-Koehler force achieves the value of the binding force between the dislocation line and solute atoms; the dislocation segment L_c (L_c is the pinning correlation length) is released. Then, the critical stress σ_c is done [29] as

$$\sigma_c = \left(\frac{n_p^2 f_p^4}{\gamma}\right)^{1/3} \quad if \quad f_p << \gamma\, n_p\, b^3, \tag{15}$$

where n_p is the density of dislocation pinning points (solute atoms or their small clusters), f_p is the elementary pinning force and γ is the dislocation elastic energy $\gamma = \kappa^- \text{ Gb}^2$ where b is the Burgers vector magnitude, κ^- is a constant of the order of 0.5. The collective pinning energy may be estimated as

$$U_c = (\gamma n_p f_p^{\,2} b^6)^{1/3}. \tag{16}$$

When the stress (strain) amplitude reaches its critical value, the dislocation motion has features typical for avalanche motion. Long free dislocation segments may operate in the slip plane and damping rapidly increases. Such collective pinning is obvious from **Figure 3a** for AX41 alloy. The critical strain (stress) for break-away of dislocations depends only slightly on the thermal treatment, that is, the microstructure is very stable due to the formation of Mg_2Ca precipitates which are more thermally stable in comparison with $Mg_{17}Al_{12}$. The constant length of shorter dislocation segments is manifested by a nearly constant C_2 parameter as it was observed in the homogenised AM20 and AX41 alloys (**Figures 2b** and **3b**).

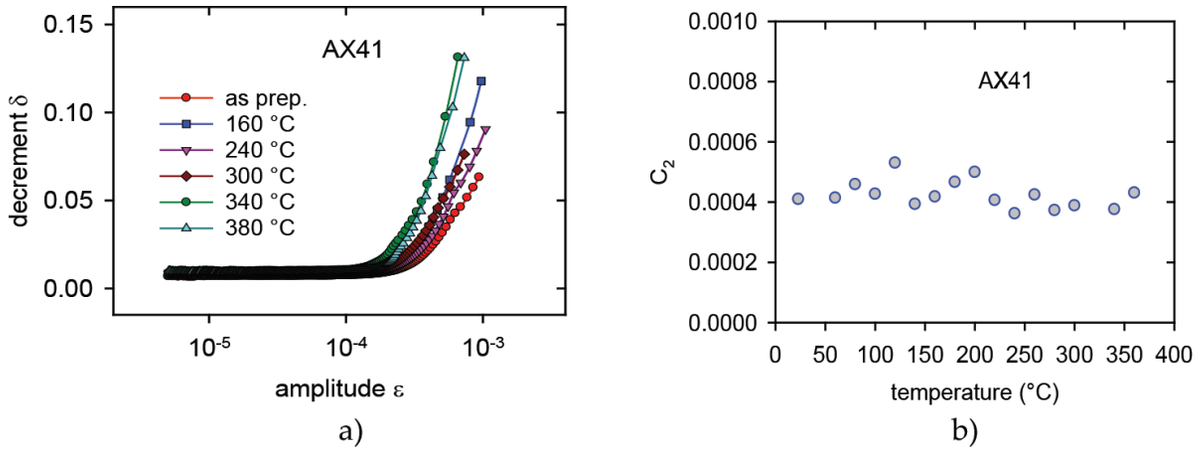

Figure 3. Amplitude dependence of decrement measured in AX41 alloy after thermal cycling (a) and temperature dependence of the C_2 parameter (b).

Different results were found in the case of an AZ31 alloy in the as-cast state (see **Figure 4a**, **b**). The alloy was thermally treated in the similar way as the AM20 alloy. ADIF measured in the as-cast sample and after the thermal cycling up to 240°C showed no changes in the microstructure (**Figure 4a**). Thermal treatment at higher temperatures influenced both the amplitude-independent as well as amplitude-dependent components of the decrement (**Figure 4b**). Both increased with increasing upper temperature of the thermal cycle. A rapid increase of the δ_0 component indicates some microstructural changes in the sample. The microstructure of the sample after the measurement series is shown in **Figure 5**. Tiny precipitates situated in the grain boundaries are the characteristic feature in the microstructure (**Figure 5**). The formation of precipitates is connected with the purification of the grains interior. A decrease of the solute atom concentration inside of grains increases the effective length of dislocation segments ℓ. The δ_0 component is very sensitive to ℓ, as it follows from Eq. (8); it means the internal friction rapidly increases in the amplitude-independent component.

http://dx.doi.org/10.5772/67028

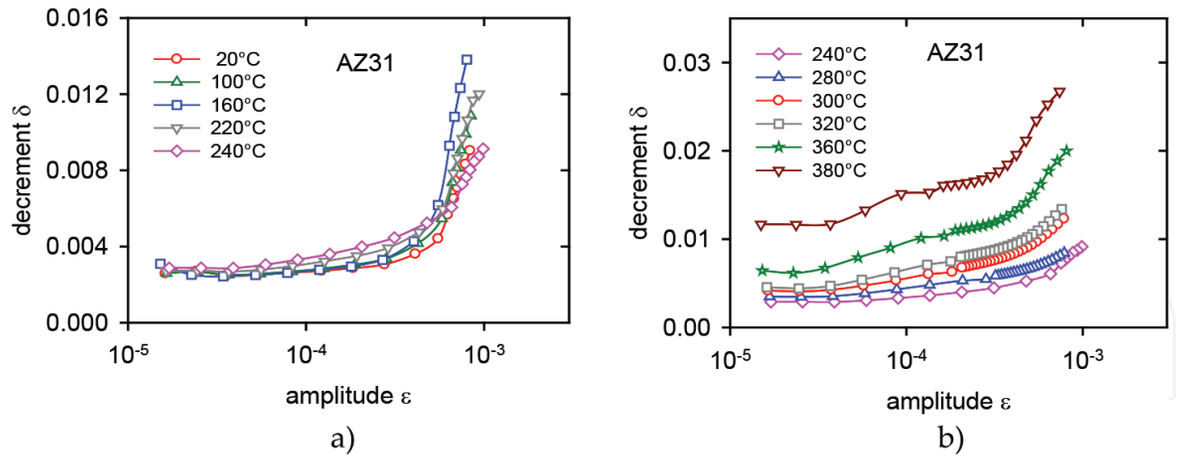

Figure 4. Amplitude dependence of decrement measured in AZ31 alloy for various upper temperatures of the thermal cycle: lower temperatures (a) and higher temperatures (b).

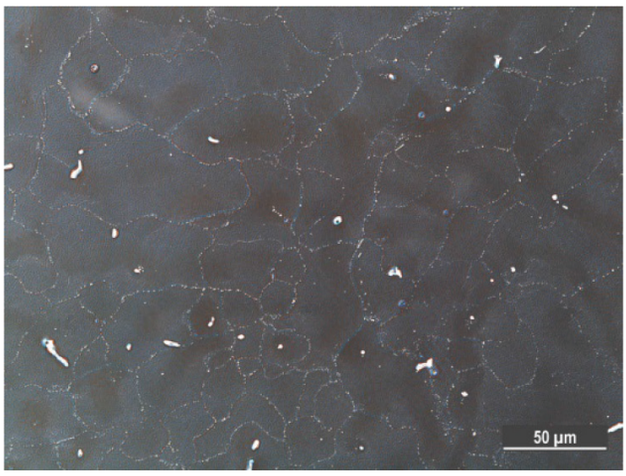

Figure 5. Microstructure of the AZ31 alloy after the thermal cycling.

2.1.1. Summary

From the ADIF investigations in AM, AX and AZ magnesium alloys, it can be concluded that changes in the microstructure of alloys may be detected using the internal friction measurement. Thermodynamic processes occurring in the alloys change the effective length of the dislocation segments. These processes take place mainly at temperatures higher than 200°C. Free solute atoms occupy the dislocation line and the stress necessary for the break-away of dislocations is very high. Avalanche release of dislocation lines (and also their length) leads to a rapid increase in the internal friction.

2.2. Magnesium alloys-based composites reinforced with short fibres

Metal matrix composites (MMCs) are materials combining two or more components with different physical and chemical properties. The commercial Mg alloys AZ91, ZC63 were reinforced by

δ-alumina short fibres (Saffil®, 3 μm in diameter with the mean length of about 87 μm) applying the squeeze-cast technology. The preform consisted of short Saffil fibres and a binder system (containing Al_2O_3 and starch). Fibres exhibited a planar isotropic fibre distribution. The preform was preheated to a temperature higher than the melt temperature of the alloy and then inserted into a preheated die. The pressure was applied in two stages. Composites based on AZ91, ZC63 alloys were exposed to the T4 heat treatment (AZ91: 413°C/18 h; ZC63: 440°C/8 h). Microstructure of the AZ91+14.6% Saffil fibres composite is introduced in **Figure 6a**. The sample was cut so that the fibres plane was parallel to the section plane. It can be seen that the distribution of fibres is not ideal and many fibres were broken during the squeeze-casting process.

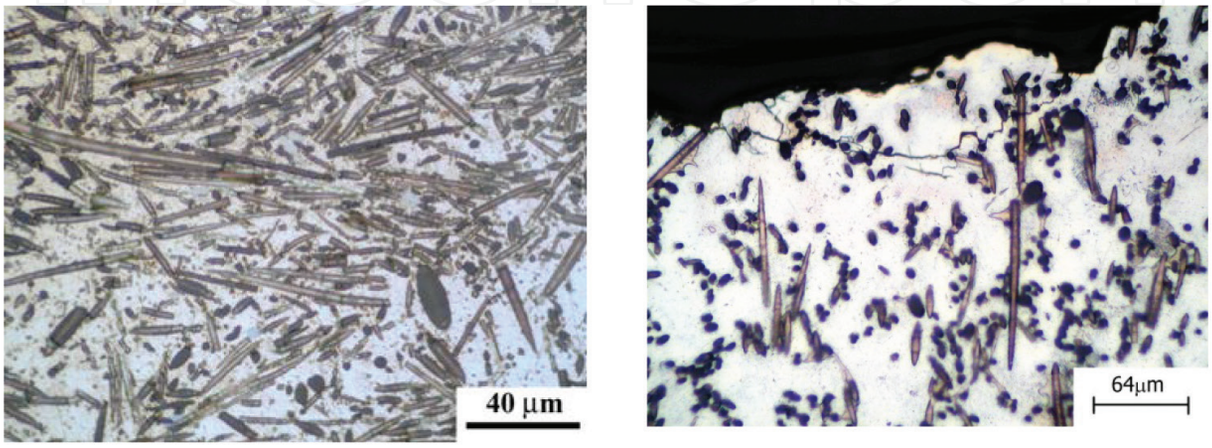

Figure 6. AZ91/Saffil composite before mechanical cycling (a) and cracks in the vicinity of the fatigue fracture plane after mechanical cycling (b).

Figure 7a shows the plots of the logarithmic decrement against the strain amplitude for the ZC63 magnesium alloy reinforced with 24.9 vol.% Saffil fibres before and after thermal cycling between room temperature and an increasing upper temperature of the thermal cycle. **Figure 7b** shows results obtained for higher temperatures. From **Figure 7a,b**, it can be seen that the strain dependencies of the logarithmic decrement exhibit two regions in good accord with Eq. (7). The values of δ_H in the strain amplitude-dependent region increase very strongly with increasing upper temperature of the thermal cycle up to 260°C, and then above 260°C, the values of δ_H again decrease with the upper temperature. Similar results were found for other composites based on magnesium alloys; only the critical temperature T_C at which the original increase of the amplitude-dependent decrement component turns to the decrease is different for various magnesium alloys. Similar results were found for the AZ91+14.9 vol.% Saffil short fibres (**Figure 8a**, **b**). The critical temperature T_C was in this case found to be 280°C. This critical temperature was found for ZC63/Al_2O_3 260°C (temperature 280°C was not measured), ZE41/ Al_2O_3 300°C. The critical temperature for QE22 was about 360°C and for AX41/ Al_2O_3 310°C, depending on the melting point of the matrix alloy.

In the lower-strain amplitude region, the decrement is only weakly dependent on the strain amplitude. In the second region, for higher strains (or stresses, according to Hooke's law they are proportional), the decrement increases strongly with increasing strain amplitude.

http://dx.doi.org/10.5772/67028

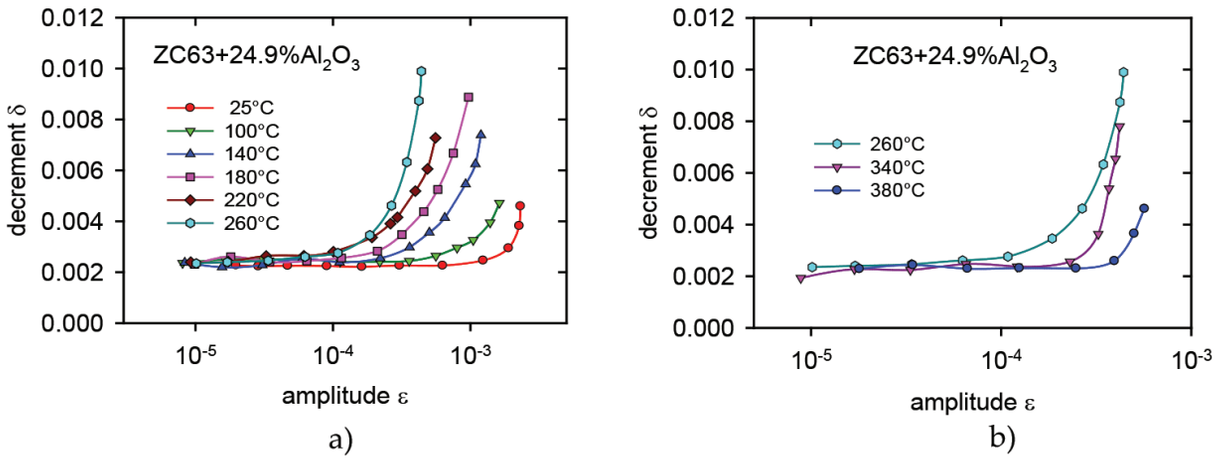

Figure 7. Amplitude dependence of decrement measured for ZC63 alloy reinforced with 24.9 vol.% of Saffil fibres after thermal cycling: lower upper temperatures of the thermal cycle (a) and higher temperatures of the thermal cycle (b).

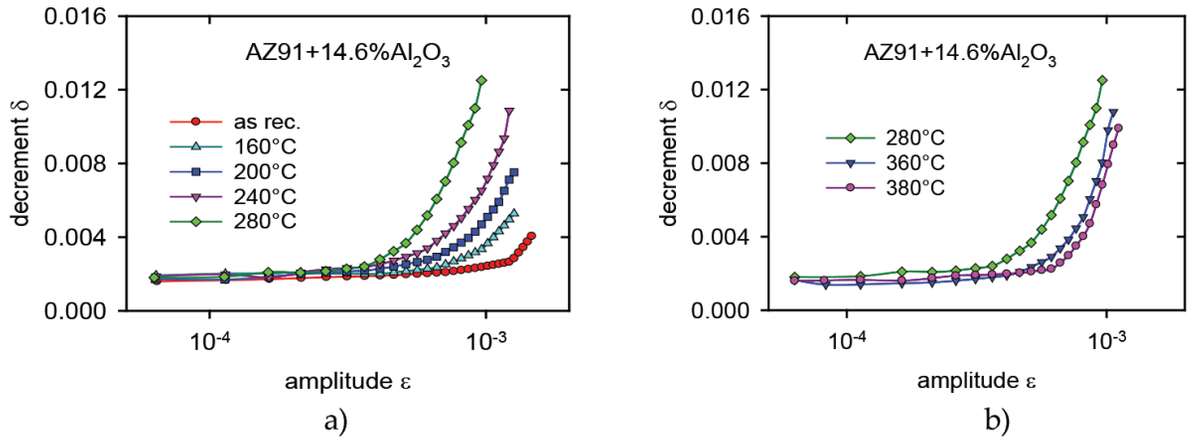

Figure 8. Amplitude dependence of decrement measured for AZ91 alloy reinforced with 14.6 vol.% of Saffil fibres after thermal cycling: lower upper temperatures of the thermal cycle (a) and higher temperatures of the thermal cycle (b).

A number of possible damping mechanisms can be identified in MMCs. Interfaces present in composites are very effective source of damping (interfacial frictional sliding, local dissipative interfacial processes and interfacial diffusion). Grain boundary sliding can occur in the same way as in the unreinforced materials. A finer grain size, which is typical for most MMCs, means that there this process may occur with the higher intensity. On the other hand, ceramic reinforcements exhibit low dislocation density, then dislocation motion and grain boundary sliding are limited; the damping effect from these mechanisms will be reduced in proportion to the remaining volume fraction of the matrix. All these effects (dislocation damping, interface and grain boundary damping) may influence the amplitude-independent δ_0 component, while the amplitude-dependent component δ_H is caused by dislocation motion in the material.

The experimental data were analysed using relationship (14). Values of the C_2 parameter are introduced in **Figure 9** for ZC63 (**a**) and AZ91 (**b**) alloys reinforced with Saffil fibres. Note that good correlation with the theory presented was found only for temperatures higher than

50–100°C. Decreasing values of the C_2 parameter with the upper temperature of the thermal cycle up to temperatures 240–260°C indicate that the length of shorter dislocation segments ℓ increases with increasing upper temperature. Further cycling at temperatures higher than 240–260°C again increased C_2 parameter, that is, the length of dislocation segments ℓ decreased.

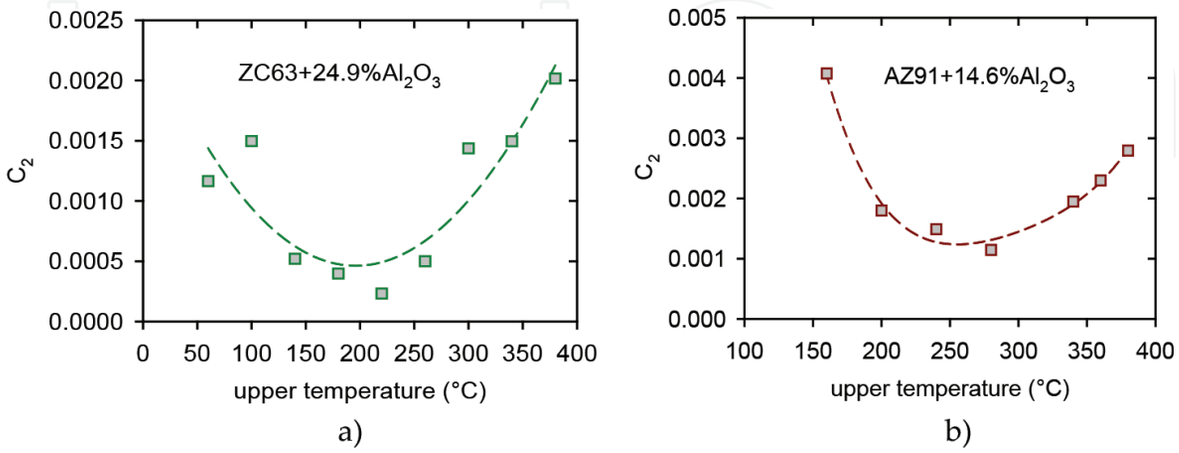

Figure 9. Temperature dependence of the C_2 parameter in the AZ63 alloy with 24.9% of Saffil fibres (a) and AZ91 alloy with 14.6% of Saffil fibres (b).

Metallic matrices and ceramic reinforcement are in the equilibrium at the manufacture temperature. Cooling to the room temperature induces thermal stresses [30]. The coefficient of thermal expansion (CTE) of ceramic reinforcement is lower than that of most metallic matrices. This means that when the composite is subjected to a temperature change, thermal stresses will be generated. Generally, these thermal stresses may be formulated in the following form:

$$\sigma_t = \mathrm{f}(C, r_i)\,\Delta\alpha\Delta T, \tag{17}$$

where f(C,r_i) is a function of the elastic constants C, and geometrical parameters r_i, $\Delta\alpha$ is the absolute value of the difference in the expansion coefficients of the components, and ΔT is the temperature change. Typically there is a large difference between the thermal expansion coefficient (CTE) of the matrix and the reinforcing phase. Even small temperature changes may generate thermal stresses. These internal stresses generated by thermal cycling of composites can be reduced by various relaxation mechanisms: dislocations production, their glide, by decohesion or sliding of the matrix-reinforcement interface, by diffusion of solute atoms in the matrix. Density of newly created dislocations created in the vicinity of the reinforcement is significantly higher than elsewhere inside of the matrix. The dislocations generated during cooling from an elevated temperature below a certain temperature T_{cr} can glide inducing plastic deformation into the matrix.

The observed results may be explained if we consider that during cooling and also during thermal cycling new dislocations are created due to the difference in the CTE. This process

may be influenced by the thermodynamic processes occurring in the matrix during the thermal cycling. Chmelík and co-workers [31] measuring the acoustic emission from the thermally treated composite (without any applied stress) have shown that new dislocations are formed in the cooling part of the thermal cycle. Higher dislocation density decreased the effective length of dislocation segments considering that the number of pinning points is constant. Number of free foreign atoms or their small clusters can be modified by thermodynamic processes in the matrix. A redistribution of solute atoms may be studied by electrical resistivity measurements. Residual resistivity ratio RRR ($RRR^{-1} = \rho_e(77\ K)/\rho_e(293\ K)$) measured for step-by-step annealed sample at increasing temperature is introduced in **Figure 10a** for ZC63/Al_2O_3 MMC. A sharp drop in RRR^{-1} detected in the temperature range from 160 to 240°C may be explained by the solute redistribution. This decrease of the resistivity reflects very complex processes; precipitates of various types can be formed in the matrix. The absence of the expected ageing effect might be due to the massive CuMgZn consuming a high amount of alloying elements. Electrical resistivity measurements have shown that the precipitation processes occur in some Mg-based MMCs approximately between 200 and 300°C [32–34]. Similarly, the matrix alloy is purified from the free solute atoms also in the AZ91 alloy as it will be shown in Section 3.3.

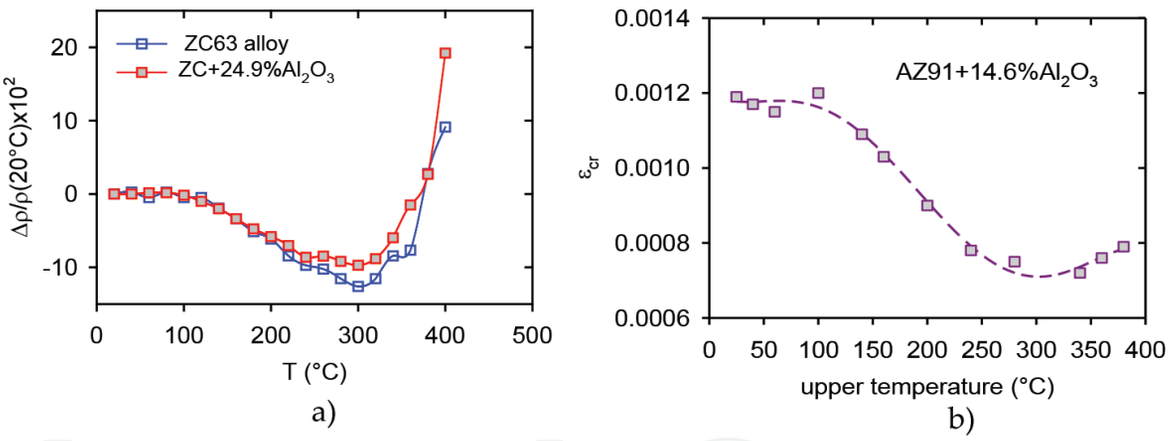

Figure 10. Temperature dependence of the residual resistivity ratio in ZC63 alloy and composite (a) and critical strain in the AZ91+14.6% of Saffil fibres (b).

From **Figure 9a**, **b**, it is obvious that the C_2 constant decreases with increasing upper temperature of the thermal cycle. This tendency finished at temperatures between 200 and 300°C (depending on the matrix alloy) and then it again increases with temperature. Such behaviour may be explained by the formation of plastic zones which may accommodate thermal stresses produced at the matrix/ceramic fibre interfaces.

The radius of this plastic zone is given by the following approximate relationship [35]:

$$r_{plz} = r_f \left[\frac{4\Delta\alpha E_M}{(5-4\nu)\ \sigma_y} . \Delta T \right]^{1/2}, \tag{18}$$

where E_f and E_M are Young's moduli of fibres and matrix, respectively, ν is Poisson constant and σ_y the yield stress in the matrix, r_f is the radius of fibres. Similarly, it is possible to express the volume fraction of the plastically deformed matrix [35]

$$f_{plz} = f\left[\frac{4\Delta\alpha\, E_M}{(5-4\nu)\,\sigma_y}.\Delta T - 1\right]. \tag{19}$$

If the volume fraction of the plastified matrix increases above a certain value, the plastic zones may overlap. In the overlapped zones, the dislocation loops formed near the interfaces have the opposite sign on both sides of the fibre. At higher temperatures, the yield stress in the matrix is lower than internal stress and at temperatures higher than 260–340°C, the tensile stresses change to compression ones. At this moment, dislocations move in the plastic zones and annihilation of dislocations can occur and hence the dislocation density decreases.

Chmelík and co-workers [31] have measured acoustic emission of samples thermally cycled between room temperature and an increasing upper temperature of the thermal cycle. At elevated temperatures from 200°C (in the case of AZ91 MMC) to 280°C, permanent elongation of the sample was detected, followed by rapid shortening of the sample after cycling at temperatures higher. These characteristic temperatures were different for various magnesium alloys used as the matrix alloys, but in each case, the critical temperature at which the sample became to be shorter accords with the critical temperature obtained in the internal friction experiments (AZ91/Al_2O_3 280°C, ZC63/Al_2O_3 260°C (temperature 280°C was not measured), ZE41/Al_2O_3 300°C, QE22/Al_2O_3 360°C). A decrease of the amplitude-dependent component of the decrement is observed in the region where the sample is plastically deformed by thermal stresses. Acoustic emission signal was detected only in the cooling parts of the thermal cycle while high-temperature strain of the sample was completely noiseless.

The temperature dependence of the critical strain ε_{cr} is shown in **Figure 10b**. All measurements were performed at ambient temperature. Thus, we can assume that parameter A and the activation energy U_1 in Eq. (11) are, in the first approximation, independent of thermal treatment. Then, the critical strain ε_{cr} depending on the length of dislocation segments ℓ follows the same tendency as the C_2 parameter.

2.2.1. Summary

Thermal stresses are generated after the thermal cycling of magnesium alloys reinforced by short Saffil fibres. These stresses may be relaxed by anelastic as well as plastic strain. Internal friction measurements can detect newly created dislocations in the vicinity of fibres ends.

Internal friction measurements showed that changes in the microstructure start at temperatures above about 200°C. Precipitation processes and solute atoms migration are responsible for these changes. Thermal internal stresses generated at temperatures higher than

220–280°C are high enough to invoke motion of newly created dislocations. Thermal cycling at temperatures higher than ~300°C causes movement and annihilation of new dislocations (which are only slightly pinned and well movable) in the matrix, under appearing compressive thermal stresses, which leads to a decrease of internal friction.

2.3. Influence of mechanical cycling on ADIF

The same composite as in Section 2.2, that is, AZ91 alloy with 14.6% of Saffil fibres, was mechanically cycled in the same apparatus in which the ADIF was measured. The sample vibrated certain number of cycles at the resonant frequency, and then the amplitude dependence of decrement was measured.

The end of the fatigue life of the sample was manifested by the rapid increase of the resonant frequency. The sample was cycled up to the sample failure. It was reached at $N = 2.19 \times 10^8$ cycles, the maximum strain amplitude was 1×10^{-3}.

The amplitude-dependent internal friction curves determined in the as-received state and after definite numbers of cycles are introduced in **Figure 11a**. A rapid increase of the decrement was observed between the first measured curve for $N = 0$ and the second measured curve after 1 min of cycling, corresponding to $N = 4.02 \times 10^3$ cycles. The logarithmic decrement estimated in the amplitude-independent region for the strain amplitude $\varepsilon = 2 \times 10^{-4}$ is shown in **Figure 11b**. A saturated region, where the decrement is more independent of the number of cycles, was found from $N = 4 \times 10^3$ to approximately 1×10^6 cycles. Further cycling led to a rapid decrease of the decrement and then again an increase followed with the fracture of the sample. A rapid increase of the amplitude-independent component of decrement δ_0 was observed for number of cycles $N = 4 \times 10^7 - 9 \times 10^7$ as it is demonstrated in **Figure 12a**. After further cycling, local maxima appeared in the amplitude-independent part of the curves as it can be seen in **Figure 12b**.

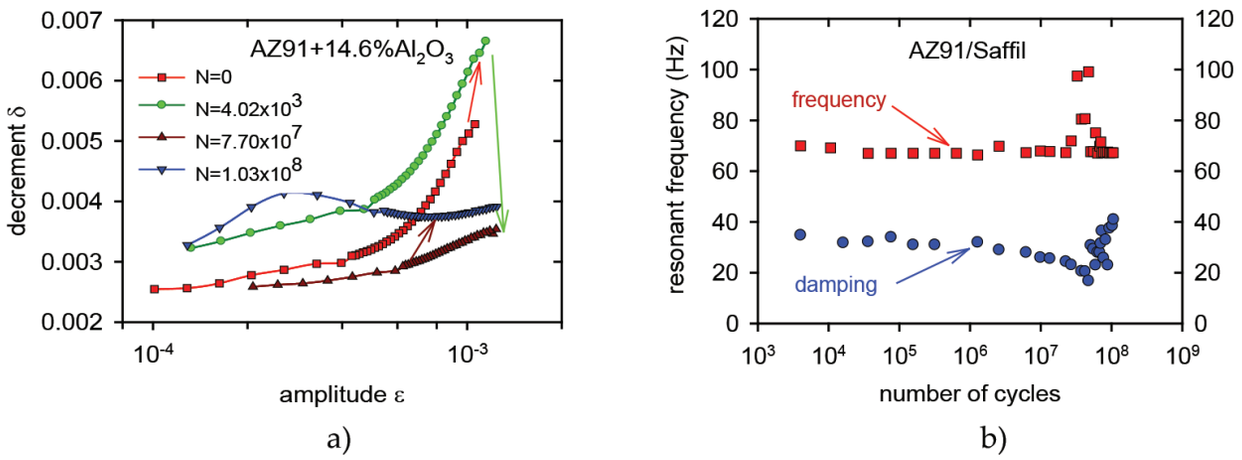

Figure 11. Strain amplitude dependences of the logarithmic decrement for as-received state and after certain number of cycles (a) and resonant frequency and damping measures after N cycles (b).

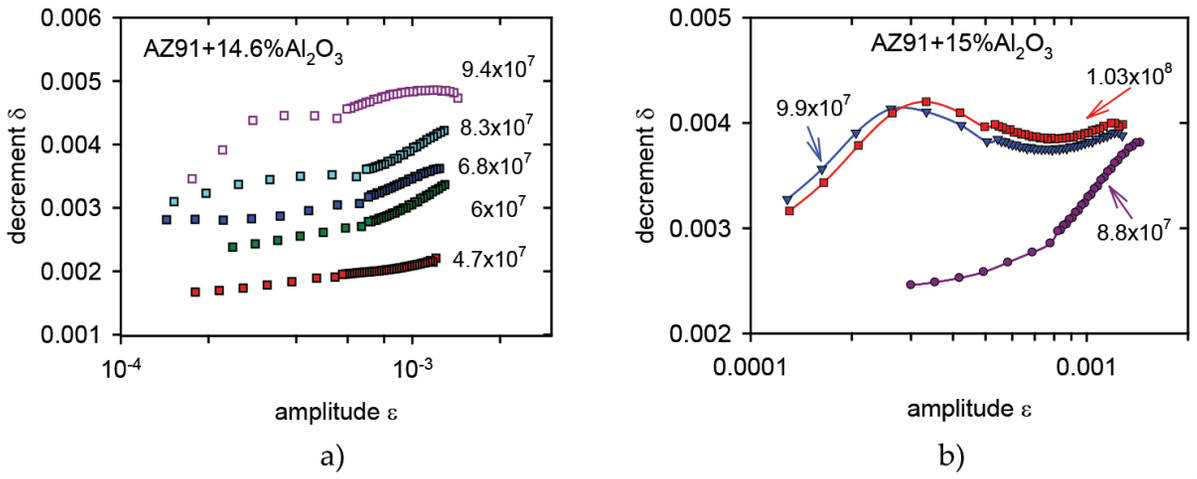

Figure 12. Rapid increase of decrement observed after cycling (a); local maximum in the amplitude independent part of decrement (b).

Changes in the composite response upon cyclic loading are primarily caused by plastic deformation in the matrix [36]. The cycling response in the material containing particles impenetrable for dislocations leads to a rapid increase in the dislocation density during cyclic loading until a saturated state is reached. Composites typically exhibit a higher dislocation density compared with their monolithic counterparts. The dislocations have to circumvent the impenetrable ceramic fibres and in the case of the AZ91 alloy also precipitates $Mg_{17}Al_{12}$. New dislocations are generated at the matrix/obstacles interfaces. According to Eq. (9), the amplitude-independent component of the logarithmic decrement depends on the dislocation density and the length of the shorter dislocation segments ℓ. The observed increase of the decrement at the onset of the cycling process is a result of the increase in the dislocation density. Because the number of the pinning points is constant and the effective length of the shorter dislocation segments ℓ is higher, the decrement increases. During further cycling, the dislocations are trapped by the interface, and induce disordered three dimensional dislocation structures with a few dislocations extending in the matrix. The density of movable dislocations is reduced. Shuttling of these dislocations accommodates the imposed strain but the damping decreases as it is obvious from **Figure 11a**, **b**. A rapid increase of the logarithmic decrement for the number of cycles higher than 4.7×10^7 (**Figures 11b** and **12a**) indicates nucleation and growth of fatigue cracks. We observed also influences of the number of cycles on the sample resonant frequency. A rapid increase of the damage parameter of the specimen after N cycles, $D(N)$, can be defined [37] as

$$D(N) = 1 - \frac{E_N}{E_o} = 1 - \frac{f_N^2}{f_o^2}, \tag{20}$$

where E_N is an effective Young's modulus of the specimen after N cycles and E_0 is Young's modulus for $N = 0$ and f_N and f_0 are the resonant frequencies of the specimen after N cycles and for $N = 0$, respectively. Microstructural investigations showed that the initiation sites of cracks were fibres, clusters of fibres and large-size precipitates (see **Figure 6b**).

A smooth local maximum in the amplitude dependence of the logarithmic decrement was observed after very high numbers of cycles (see **Figures 11a** and **12b**). This maximum is caused by the formation of cracks in the fatigued matrix. A simple rheological model taking into account the crack origin of damping was developed by Göken and Riehemann [38]. According to the model, one elementary crack is assumed to be represented by a frictional grip that is attached in series to a spring E_1 representing the loss of modulus due to opening of the crack. This frictional grip is absolutely firm for stresses lower than its critical stress $\sigma<\sigma_{ci}$. In this stress region, the spring E_1 and frictional grip σ_{c1} attached parallel to another spring E_r are elongated by an amount of ε_{c1} with $\sigma_{c1}=(E_r+E_1)\varepsilon_{c1}$. The grip is separated at $\sigma=\sigma_{c1}$ where the spring E_1 is released and the strain increases according to $\sigma_{c1}=E_r\varepsilon$ because only E_r representing the relaxed modulus is elongated. In this process, the elementary crack opens at the critical strain and the mechanical energy ΔW is converted to heat by the displacement of the two crack surfaces, by emission of dislocations at the crack tips, or by crack growth. The mechanical loss can be written as

$$\eta = \frac{1}{2\pi}\frac{\Delta W}{W} \cong \frac{E_i}{E_r}\left(\frac{\sigma_c}{\sigma}\right)^2 \propto \left(\frac{\varepsilon_c}{\varepsilon}\right)^2 \tag{21}$$

for $\varepsilon\geq\varepsilon_c$ and $\eta = 0$ for $\varepsilon<\varepsilon_c$. Introducing n combinations of grips σ_{ci} and springs E_i with $I = 1\ldots n$, the damping behaviour of n cracks can be modelled. The local maximum in the amplitude dependence of the logarithmic decrement was caused by the distribution of cracks length and their orientations leading to a nearly continuous distribution of the critical strains σ_c. All occurring local maxima could be fitted with good accuracy when a lognormal distribution of critical stresses σ_c was assumed. In **Figure 12b**, the local maximum after 9.9×10^7 cycles is shifted to slightly higher damping and higher strain amplitude after additional cycles leading to a total number of 1.02×10^8 cycles. This may indicate that new smaller cracks are created or dislocation damping increases again during this period. The latter could already be observed in the high amplitude region from 8.8×10^6 to 9.9×10^7cycles. Fatigue cracks were found after mechanical cycling in the composite microstructure as it is demonstrated in **Figure 6b**.

2.3.1. Summary

Fatigue can successfully be studied by the measurement of strain amplitude-dependent damping after increasing numbers of mechanical cycles. For mechanical cycling of AZ91/Saffil composite mainly dislocation effects could also be found for cycle numbers up to 4.7×10^7. For further cycling, a strong increase of damping can be attributed to nucleation and growth of cracks leading to fracture of the sample. Smooth relative maxima appearing on the damping versus strain curve can be explained and evaluated by a rheological model of the effect of cracks on damping.

2.4. Magnesium zirconia nanocomposite

Magnesium with 3 vol% of zirconia nanoparticles was prepared by powder metallurgical route. Powder from Mg was mixed with ZrO_2 nanoparticles (the mean size of 14 nm) and milled together for 1 h in a planetary ball mill. The mixture was subsequently pre-compressed followed

by hot extrusion at a temperature of 350°C under a pressure of 150 MPa. After extrusion, the originally more or less equiaxial grains changed into elliptical grains with the long axis parallel to the extrusion direction. The grain size in the cross section was about 3 μm and in the extrusion direction 10 μm. ADIF was measured after mechanical cycling at room temperature. Experiments were performed in similar way as in the case of AZ91/Saffil composite. Decrement estimated for two strain amplitudes depending on the number of cycles is shown in **Figure 13a**.

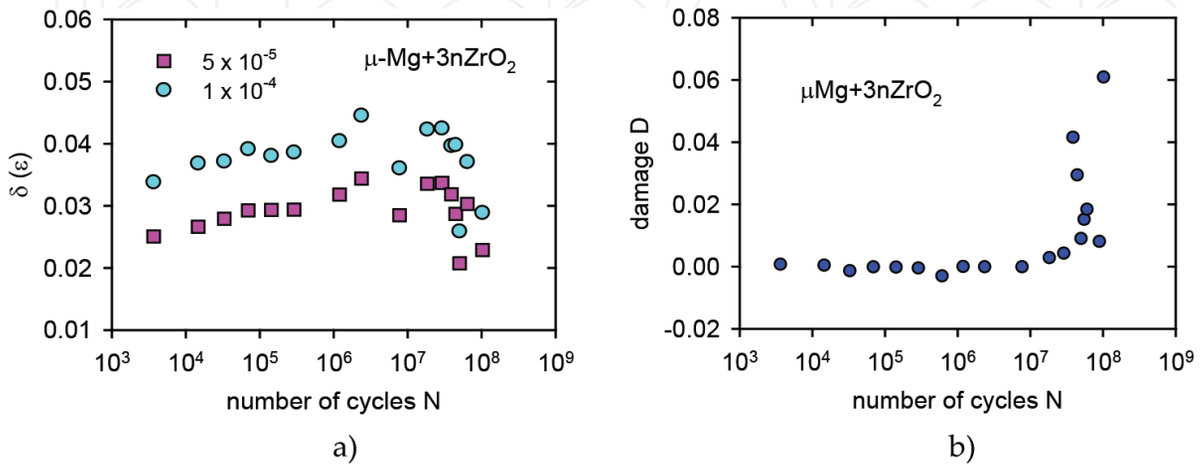

Figure 13. The logarithmic decrement measured for two amplitudes depending on number of cycles (a) and damage parameter versus number of cycles (b).

Mechanical cycling in the region from 3×10^3 to 2.4×10^6 leads to the decrement increase. Observed increase of decrement is very probably a consequence of the dislocation density increase and also an increase of the effective length between weak pinning points. Further cycling up to 2.9×10^7 cycles decreased the decrement. This drop is caused by a decrease of the dislocation density, which is a consequence of interactions between dislocations. The higher dislocation density limited the slip length of vibrating dislocation segments. Rapid increase of the decrement is caused by the cracks creation. Rapid decrease of the damage parameter shown in **Figure 13b** observed for the number of cycles of $N>10^7$ and the decrease of the resonant frequency at the end of the fatigue process indicates loss of the stiffness as a consequence of the creation and propagation of cracks.

2.4.1. Summary

Magnesium zirconia nanocomposite was cycled at room temperature and after certain number of cycles the logarithmic decrement was measured. Plastic deformation during cycling increased the dislocation density and also the measured decrement. The loss of stiffness at the end of the fatigue process is a consequence of the cracks formation and propagation.

2.5. Ultra-fine-grained magnesium

Ultra-fine-grained magnesium (UFG-Mg) samples were prepared by ball milling of powder in an inert atmosphere and subsequent consolidation and hot extrusion. The linear grain size

http://dx.doi.org/10.5772/67028

of specimens estimated by X-ray line profile analysis was about 100–150 nm. Samples were cyclically loaded until failure with bending vibrations in the apparatus also used for damping measurements. The resonant frequency of the system ranged from 59 to 62 Hz. The end of the fatigue life of a sample was manifested by a rapid decrease of the resonant frequency. The sample was cycled up to failure, which was reached at $N = 2.74 \times 10^8$ cycles.

The amplitude-independent component, δ_0, and the damping value at the maximum amplitude, δ_{max}, plotted against the cycle number are shown in **Figure 14a**. It can be seen that the decrement is more or less constant at the onset of the cycling process. Cycling in the region between 10^7 and 10^8 cycles leads to an increase of the decrement. The observed increase of the decrement indicates a rapid increase of the dislocation density and also an increase in the distance between weak pinning points. This increase of the decrement, on the other hand, is accompanied by a decrease of the resonant frequency. **Figure 14b** shows the damage D (defined by Eq. (20)) plotted against the cycle number N. A rapid increase of D occurred for $N > 10^8$. The measured decrease of the resonant frequency at the end of fatigue process indicates a stiffness loss due to the formation of cracks and may also be caused by an increase of the number of bowable or moveable dislocations as a function of cycling. A rapid increase of the amplitude-dependent component of the decrement at the end of the sample life is due to rapid nucleation or growth of cracks and a resulting strong local increase in the free dislocation density. Newly created dislocations at cracks tips accommodate these stresses.

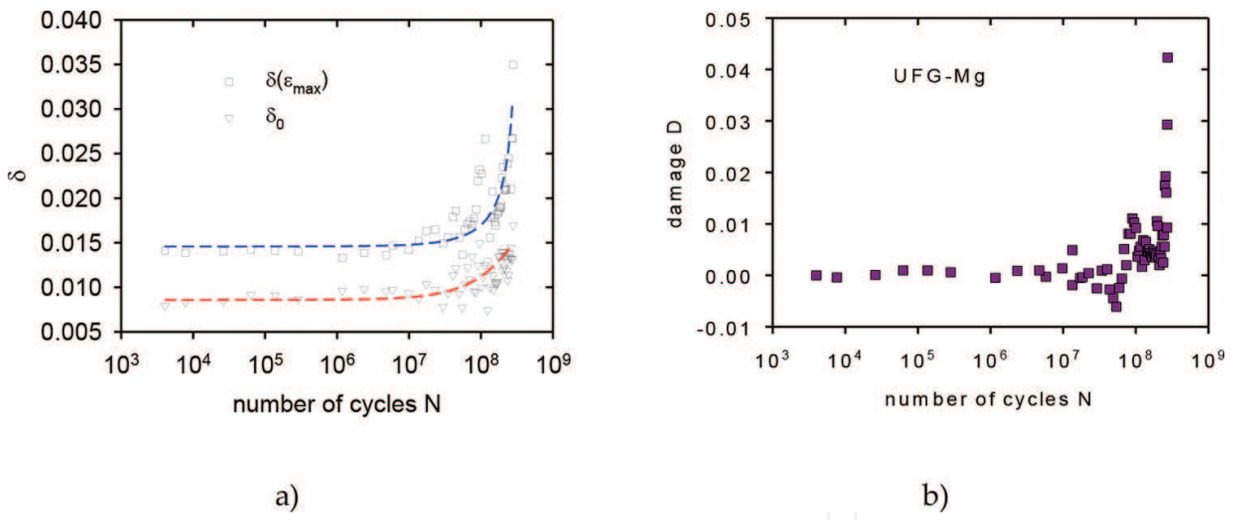

Figure 14. Amplitude dependence of decrement measured in UFG-Mg for two amplitudes (a); damage parameter depending on the number of cycles (b).

2.5.1. Summary

The accumulation of plastic deformation mainly due to an increase of the dislocation density is the significant feature of the fatigue process. Cycling higher than 10^8 cycles led to nucleation and growth of cracks. Newly created and propagated cracks increased the logarithmic decrement and damage parameter.

3. Temperature relaxation spectrum of internal friction

3.1. Microcrystalline Mg

Microcrystalline magnesium was prepared using the powder metallurgical route. The temperature dependence of the loss angle tan φ estimated over a wide range from room temperature up to 480°C is given in **Figure 15a** for three measuring frequencies of 0.5, 5 and 50 Hz. Two peaks showing different intensities have been found: the weak low-temperature peak and the more intense high-temperature peak. It can be seen that both peaks shift to a higher temperature with increasing frequency, indicating that they may be relaxations peaks. Positions of peaks in the temperature scale are for three measuring frequencies introduced in **Table 1**. The curves shown in **Figure 15a** were measured during one heating course in the multi-frequent mode. Repeating of the thermal measuring cycles did not change the height and position of peaks. The internal friction peaks are assumed to be imposed by a background IF_b expressed by

$$IF_b = A + B\exp\left(\frac{-C_b}{kT}\right), \tag{22}$$

where k is the Boltzmann constant and T is the absolute temperature, A, B and C_b are constants. After subtracting the background by using a fitting programme PeakFit, the maximum temperature T_P was estimated for both the relaxation peaks. Exact temperatures of both peaks estimated for various frequencies are given in **Table 1**. The peak widths are broader than that for a Debye peak, characterised by single relaxation time. The internal friction peak appears at the condition $\omega\tau = 1$ [39], with

$$\omega\tau = \omega\tau_0 \exp\left(\Delta H/kT\right), \tag{23}$$

where ω is the angular frequency ($=2\pi f$, f is the measuring frequency), τ is the mean relaxation time, τ_0 the pre-exponential factor, and ΔH is the mean activation enthalpy. **Figure 15b** shows the semilogarithmic plot of the frequency versus reciprocal value of the peak temperature T_P—the so-called Arrhenius plot.

From the slope and intercept of the straight line, the mean activation enthalpy ΔH for the low-temperature peak has been obtained and its value is 1.02 ± 0.05 eV. Internal friction in magnesium has been studied by several authors. Their results are summarised in **Table 2**. The peaks found above room temperature up to 100°C were described to dislocation effects. As far as the peak observed may have a dislocation nature, prestraining of the sample at a low temperature should influence the height of the peak. Deformation by rolling at room temperature ($\varepsilon \approx 2\%$) increased the strength of the low-temperature peak. This result is different from an estimation presented in the paper [14], where probably the identical peak P_D vanished after annealing at 570 K. Similar peak was found by Trojanová and co-workers [40, 41] for ultra-fine-grained magnesium prepared by ball milling and hot extrusion.

In the case of a relaxation processes linked to dislocation motion, the activation area $A = V/b$ (b is the Burgers vector and V activation volume) is the area that a dislocation has to move in order to activate the process, this means to overcome the barrier. Therefore, the product $V\sigma^*$

http://dx.doi.org/10.5772/67028

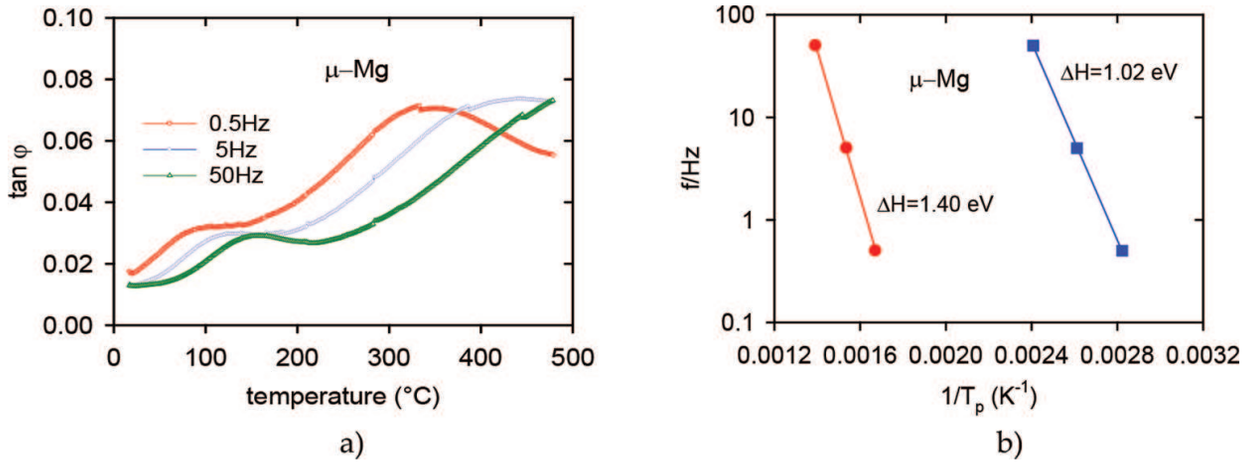

Figure 15. Temperature dependence of the loss angle measured at three frequencies (a) and Arrhenius plots constructed for low- and high-temperature peaks (b).

f/Hz	*P*1 (°C)	*P*2 (°C)
0.5	84.7	325
5	133.9	377.4
50	142.2	445.2

Table 1. Peak temperatures observed for various frequencies.

Material	*T* (°C)	*f* (Hz)	Δ*H* (eV)	References
Mg99.999%	76.8	1–2		Seyed Reihani [42]
Mg99.97%	219.8	0.46		Kê [4]
Mg99.9999%	67	1		Nó et al. [14]
Mg99.9999%	157	1		Nó et al. [14]
High purity Mg	146.8			Fantozzi et al. [43]
Mg99.9999%	148.8	1	1.00	Nó [44]
μ-Mg	84.8	0.5	1.02	This work
μ-Mg	325	0.5	1.40	This work
UFG-Mg	102	1	0.95	Trojanová et al. [40]
UFG-Mg	358	1	1.77	Trojanová et al. [40]
UFG-Mg+3nGr	78	1	1.08	Trojanová et al. [45]

Table 2. Occurrence of the internal friction peaks in magnesium prepared by various routs .

represents the work done by the applied stress to promote the dislocation motion over the local barrier. Neglecting the entropy term, the activation volume can be expressed as

$$V = -\frac{\partial \Delta H}{\partial \sigma} = -k \ln(\omega\tau_0) \frac{\partial T_p}{\partial \sigma}, \quad (24)$$

using Eq. (23) and the condition $\omega\tau = 1$ for peak appearance. **Figure 16a** shows the internal friction spectrum measured at different strain amplitudes ε (from 8.3×10^{-5} to 2.3×10^{-4}). As the strain amplitude increases the peak shifts towards higher temperatures and its height increases while the background increases moderately. Taking for $\ln(\omega\tau_0) = -31.33$ ($\tau_0 = 7.9 \times 10^{-15}$ s, $\omega = \pi$ Hz), and for $\partial T_p/\partial\sigma = (1/E)1.84 \times 10^4$ (linear regression from **Figure 16b**, $\sigma = E\varepsilon$, E is the Young modulus), we obtain for the activation volume $V(\text{exp}) = 1.5 \times 10^{-28}$ m^3 and dislocation activation volume $V_d = \psi V_{exp} = 7.2 \times 10^{-28}$ m^3 = 22 b^3 (E = 42 GPa, and the Taylor factor ψ = 4.8). Considering geometrical interpretation of the activation volume

$$V = bd\,\ell_D = bA, \quad (25)$$

where the energy barrier has a width d. ℓ_D is the length of the dislocation segment between barriers. Parameters of the thermally activated process (activation enthalpy and activation volume) are typical for certain barriers and their experimental estimation gives a possibility to identify the main barriers relevant for dislocation motion. Usually, the thermally activated process is studied in plastic deformation. On the other hand, the inelastic behaviour of metallic materials can be considered as the thermally activated dislocation motion.

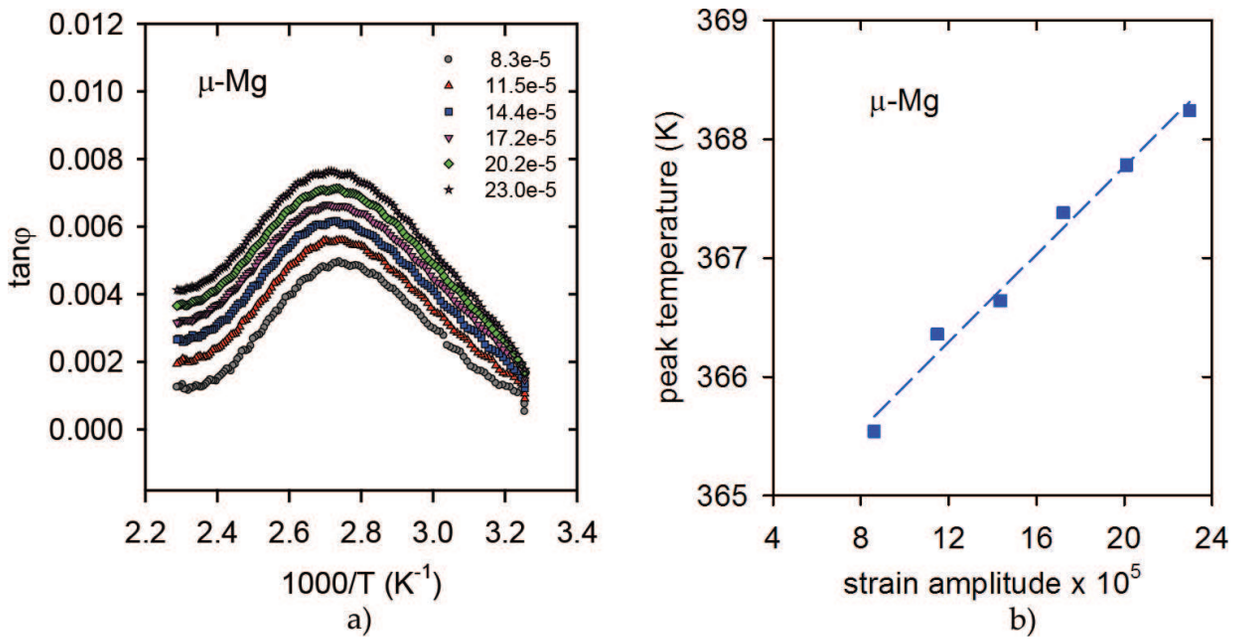

Figure 16. Temperature dependence of the low-temperature peak measured for various strain amplitudes (a) and amplitude dependence of peak temperatures (b).

The main deformation mode in magnesium is basal slip of <a> dislocations. The secondary conservative slip may be realised by <a> dislocations on prismatic and pyramidal planes of the first kind. Couret and Caillard studied by TEM prismatic glide in magnesium in a wide temperature range [46, 47]. They showed that the screw dislocations with the Burgers vector of $\frac{1}{3}$ $[11\bar{2}0]$ are able to glide on prismatic planes and their mobility is much lower than the mobility of edge dislocations. The deformation is controlled by thermally activated glide of these screw dislocation segments. A single controlling mechanism has been identified as the Friedel-Escaig mechanism. This mechanism assumes a dissociated dislocation on a compact plane (0001) that joins together along a critical length L_r producing double kinks on non-compact plane. The activation energy for this process is

$$U = 2U_K + 4U_C + 2U_R \tag{26}$$

where $2U_K$, $4U_C$ and $2U_R$ are the formation energies of the kink pair, of the four constrictions and of the two recombined segments, respectively. The activation area is proportional to the critical length between two kinks and it should be small.

$$A \propto L_r b. \tag{27}$$

The theoretical prediction leads to a value of $2U_K$ superior to 1.2 eV and to an activation area of about 15 b^2. This mechanism should give an internal friction peak similar to the Bordoni relaxation. The Friedel-Escaig mechanism is also sometimes called as pseudo-Peierls mechanism. Additionally, in this model the maximum of the internal friction peak must increase with increasing oscillating stress (strain amplitude) from a certain critical value. Thus, the comparison between the theoretical predictions and the experimental results leads to the conclusions that the observed relaxation is very probably pseudo Bordoni relaxation based on glide of screw dislocations on non-compact planes controlled by the Friedel-Escaig mechanism.

The high-temperature peak has been observed at temperature ~325°C (0.5Hz). The cold prestraining of the sample did not affect the strength of the high-temperature peak. Position and height of the peak are very stable during heating as well as cooling. The activation energy was obtained from the frequency dependence of the peak temperature (Arrhenius plot) to be 1.40 ± 0.05 eV (see **Figure 15b**). Existence of the high-temperature peak in magnesium has been reported by Kê [4] and other authors [5, 6, 10, 11]. They described this peak as being related to the grain boundary relaxation. Grain boundary sliding is realized by the slip and climb (providing a maintenance of vacancy sources and sinks) of grain boundary dislocations. Since both modes of dislocation motion must occur simultaneously, the slower one will control the grain boundary sliding. The climb mode involves jog formation and grain boundary diffusion and both modes may be affected by the interaction with impurities segregated in grain boundaries. According to ref. [48], grain boundary dislocation segments vibrate under applied cyclic stress, restoring force K is assumed to be from the elasticity of the limiting grains at triple junctions. According to this theory, the relaxation strength is for small grains not depending on the grain size:

$$(\tan\varphi)_{\max} = \frac{G\rho_s b^2}{C}, \tag{28}$$

where ρ_s is the dislocation grain boundary surface density (total dislocation length per unit of grain boundary area), G is the shear modulus and C is a constant. The relaxation time in this model is

$$\tau = \frac{kT}{b^2 C_j D K} \exp\left(\frac{\Delta H_j + \Delta H_{GB}}{kT}\right) = \tau_0 \exp\left(\frac{\Delta H}{kT}\right), \tag{29}$$

where C_j is the linear density of jogs along the dislocation line, D is the diffusion coefficient, ΔH_j, ΔH_{GB} are the activation enthalpies for the jog formation and the grain boundary diffusion, respectively. The activation enthalpy for grain boundary diffusion in the coarse-grained magnesium is 0.95 eV [49]. Comparing with the estimated activation enthalpy value of 1.40 eV, the possible jog formation energy should be approximately 0.45 eV, which seems to be a reasonable value. Similar peaks describing the grain boundary sliding are introduced in **Table 2**. Peak observed by Kê [4] was found at 219.8°C and by Trojanová [41] at 358 °C. This is very probably due to the fact that microcrystalline and ultra-fine magnesium were prepared by milling in the protective Ar atmosphere containing 1% of oxygen. MgO particles in the grain boundaries together with the alumina nanoparticles may influence grain boundary diffusion characteristics.

3.1.1. Summary

Microcrystalline magnesium was prepared by milling and hot extrusion. Internal friction was measured as a function of temperature with three frequencies 0.5, 5 and 50 Hz. Two relaxation peaks were observed: a peak at 85 (0.5 Hz) with activation energy of 1.02 eV, and a peak at 325°C (0.5 Hz) with activation energy of 1.40 eV. The estimated small values of the activation volume and the peak sensitivity to the stress amplitude lead us to conclude that the low-temperature peak is due to the screw dislocation motion on the prismatic plane controlled by the Friedel-Escaig mechanism. Grain boundary sliding is probably the reason for appearing at the high-temperature peak.

3.2. Mg-Gr nanocomposite

The Mg with 3 vol% of Gr nanoparticles was prepared by the similar procedure as the microcrystalline Mg (see Chapter 3.1). The Mg micropowder with a median particle diameter of about 40 μm was mixed for 8 h with 3 vol.% of graphite powder and milled for 8 h in the planetary ball mill in a sealed argon atmosphere. The composite was encapsulated in an evacuated Mg container, degassed at 350°C, and extruded by the preheated (350°C) 400 t horizontal extrusion press. The material was studied in a transmission electron microscope; the mean grain size of the material was found to be about 200 nm. Temperature relaxation spectra of internal friction were measured in a DMA 2980 (TA Instruments) apparatus while heating and cooling. In a temperature range from room temperature up to 480°C, the measurements were performed in the multi-frequency mode at three frequencies 0.5, 1 and 2 Hz. Throughout the measurements, the strain amplitude was 1.2×10^{-4}. The heating as well as cooling rate was 1 K/min. No grain growth during heating up to 480°C was observed.

http://dx.doi.org/10.5772/67028

Figure 17a shows the temperature dependence of the mechanical loss angle tanφ measured at three frequencies during first heating sub-cycle. Two types of peak have been found: the weak low-temperature peak and the more pronounced two high-temperature peaks. While the low-temperature peak position in the temperature scale depends on the measuring frequency, position of both high-temperature peaks does not depend on the frequency. **Figure 17b** shows the temperature dependence of mechanical loss angle measured during cooling. It is seen that the two high-temperature peaks developed into one peak. Position of this peak is not depending on frequency and it remained constant in the next heating-cooling cycles. The low-temperature peaks extracted from the internal friction spectrum subtracting the background damping are introduced in **Figure 18a**, **b** which shows the Arrhenius plot for the low-temperature peak. An estimated activation enthalpy of 1.08 ± 0.05 eV is close to activation enthalpies found for μMg and UFG-Mg as it is given in **Table 2**. This fact and together with found peak temperature from a range of 67–102°C indicates that the low-temperature peak is due to the reversible screw dislocation motion on the prismatic plane controlled by the Friedel-Escaig mechanism as it was described in paragraph 3.1.

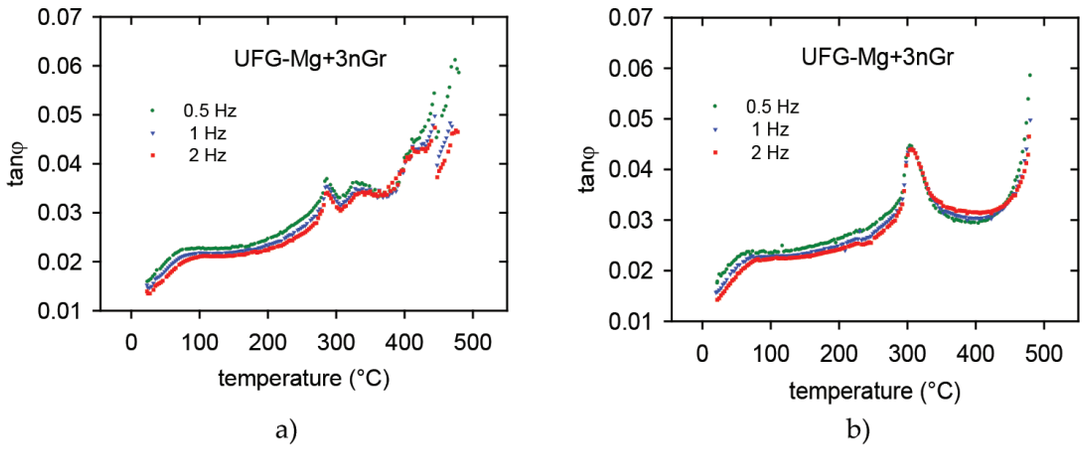

Figure 17. Temperature relaxation spectrum of internal friction measured for three frequencies while heating (a) and cooling (b).

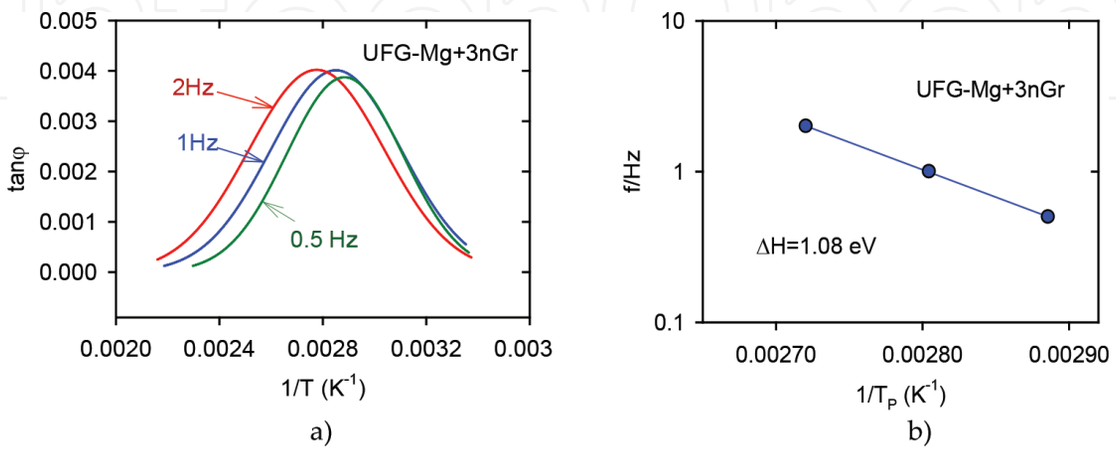

Figure 18. Subtracted low-temperature peaks (a), Arrhenius plot and activation enthalpy obtained for the low-temperature peak (b).

Observed independence of the high-temperature peak on the frequency indicates that this peak has no Debye nature. Its existence is due to newly created dislocations and their motion. An increase in the dislocation density near reinforcement with the different CTE compared with the matrix has been calculated according to Arsenault & Shi [50]

$$\rho = \frac{B V_f \Delta\alpha \Delta T}{b\left(1 - V_f\right)} \frac{1}{t_{\min}}, \tag{30}$$

where V_f is the volume fraction of the reinforcing phase, $t_{\min}$ its minimum size, b the magnitude of the Burgers vector of dislocations, B a geometrical constant, $\Delta\alpha$ the absolute value of the CTE difference between the matrix and the reinforcement, ΔT the temperature difference. Rawal [51] studied the interface in the cast Mg-Gr composite. He found, using the transmission electron microscopy, enhanced dislocation density near the interface. Dislocations were generally linear and corresponded to available basal slip systems in hcp Mg matrix. Dislocation density measurements made using the weak beam imaging technique indicate an average dislocation density of $1.6 \times 10^{13} – 6 \times 10^{14}$ m^{-2}. High density of dislocations may be attributed to the residual stress state generated because of differential contraction between the Gr and matrix during the fabrication process. In the Mg/Gr composite studied in the present work, the CTE value of high purity Mg matrix is 26×10^{-6} K^{-1} and that of the Gr is approximately 4.0×10^{-6} K^{-1} (the value for carbon fibres is $–1.4 \times 10^{-6}$ K^{-1} [52]). It is expected that such large difference could generate a high density of dislocations during heating as well as cooling of Mg/Gr system. The residual strain, or strain accumulation, produced by the thermal mismatch may be calculated from

$$\varepsilon = \Delta\alpha\Delta T. \tag{31}$$

In the absence of thermal stresses, the vibrating dislocation segments do the dislocation damping IF_d. If the composite material is heated, compressive thermal stresses σ_{th} are generated in the matrix and induce a long-range movement of dislocation, which is superimposed on the oscillatory motion induced by the apparatus. Several models are reported in the literature to describe the mechanism(s) responsible for damping in composites due to dislocation motion in the vicinity of reinforcing phase. Mayencourt and Schaller [24] have reported a non-linear dependence of the internal friction in MMCs with the cooling rate, measuring frequency and strain amplitude. Dislocation motion near the interface is controlled by the solid friction mechanism and break-away of dislocation from solutes. Vincent and co-workers [53] developed a model where a coupling between the thermal-induced strain and the alternating shear stress of the apparatus is considered. Carreño-Morelli and co-workers [25] developed a model based on the growing plastic zones around the reinforcement. Wei et al. [54] studied internal friction in Al with Gr particulates. An internal friction peak was found at about 260°C. The internal friction peak is attributed to the thermal dislocations, the thermal stress coupled to the exciting stress, and the interaction between the dislocations and the cyclic applied stress.

3.2.1. Summary

Mg with 3 vol.% of Gr nanoparticles prepared by milling and hot extrusion has been characterised by mechanical spectroscopy during continuous heating as well as cooling. Internal

friction was measured as a function of temperature with three frequencies ranging from 0.5 to 2 Hz. Two internal friction peaks were observed in the temperature relaxation spectrum. The peak observed in the vicinity of ≈ 80°C, having the activation energy of 1.08 eV, has been described to the reversible screw dislocation motion in the Mg grains on the prismatic plane controlled by the Friedel-Escaig mechanism. Thermal stresses generated due to thermal mismatch during heating as well as cooling are very probably the reason for the peak observed at ≈ 300°C. Position of this peak is insensitive to the measuring frequency. Increased dislocation density induced by thermal stresses and movement of dislocations under the thermal stress as well as the applied stress is the reason for the existence of this peak.

3.3. AZ magnesium alloys

TDIF was measured in cast magnesium alloys AZ31, AZ63 and AZ91 after homogenisation treatment (22 h at 390°C). The resonant frequency and damping analyser (RFDA) was used to determine the damping and resonant frequency. The measurements were performed in a wide temperature range from room temperature up to 400°C. The prism-shaped samples 75 × 20 × 10 mm^3 were excited to vibrations in the resonant frequency using a small striker. Damping of the sample-free vibrations was registered with a microphone and processed using special software. The resonant frequency exhibiting ~8 kHz was estimated by means of Fourier transform. The linear heating rate was chosen in the range from 1 to 4 K/min. The AZ alloys are formed by the solid solution of Al and Zn atoms in Mg (δ-phase) and the $Mg_{17}Al_{12}$ intermetallic compound (γ-phase). Precipitates existing in these alloys may be of two kinds: discontinuous precipitate (DP), which is formed by lamellae $\gamma + \delta$, and continuous precipitate (CP) having usually a form of small discs or spheres. Microanalysis of all three alloys showed the presence of the γ-phase in the AZ31 alloy while the discontinuous precipitate was observed only rarely. In the AZ63 alloy, electron compound $Mg_{17}Al_{12}$ was found beside discontinuous precipitate. AZ91 alloy exhibits similar microstructure as AZ63 alloy, only with the different proportional representation of individual phases.

The temperature dependences of the logarithmic decrement measured at the heating rate of 2 K/min for AZ31, AZ63 and AZ91 alloys are introduced in **Figure 19a**. The temperature dependence of the logarithmic decrement was measured in the AZ91 sample after the homogenisation treatment while heating is introduced in **Figure 19b**. The heating rate was 60 K/h, the cooling rate was not controlled. The temperature record showed the linear decrease of temperature up to 120–140°C. When room temperature was reached, a new measurement was started. The measurements were repeated three times. It is obvious from **Figure 19b** that the decrement is more or less constant up to approximately 220°C, and then it increases with increasing temperature. At temperature ~320°C, a local maximum of the logarithmic decrement is observed. The height of this maximum decreases in the second and third run of the measurement. The position of maximum in the temperature axis is the same for all runs.

The temperature dependence of the logarithmic decrement was measured for three heating rates as it is shown in **Figure 20a**. Note that before each measurement, a new homogenisation treatment was performed. Only the first runs of the measurements are given in **Figure 20a**. The higher heating rate, the higher temperature of the local maximum is observed. The height of the maximum simultaneously decreases with the increasing heating rate. To reveal the physical nature

of the observed local maximum in the temperature dependence of the logarithmic decrement, a sample with the smaller thickness was tested. Maximum position in the temperature scale was not shifted for the measurement with the resonant frequency of ~7 kHz (see **Figure 20b**). This fact indicates that the observed maximum is not of the Debye type. Some transitory effects must be considered.

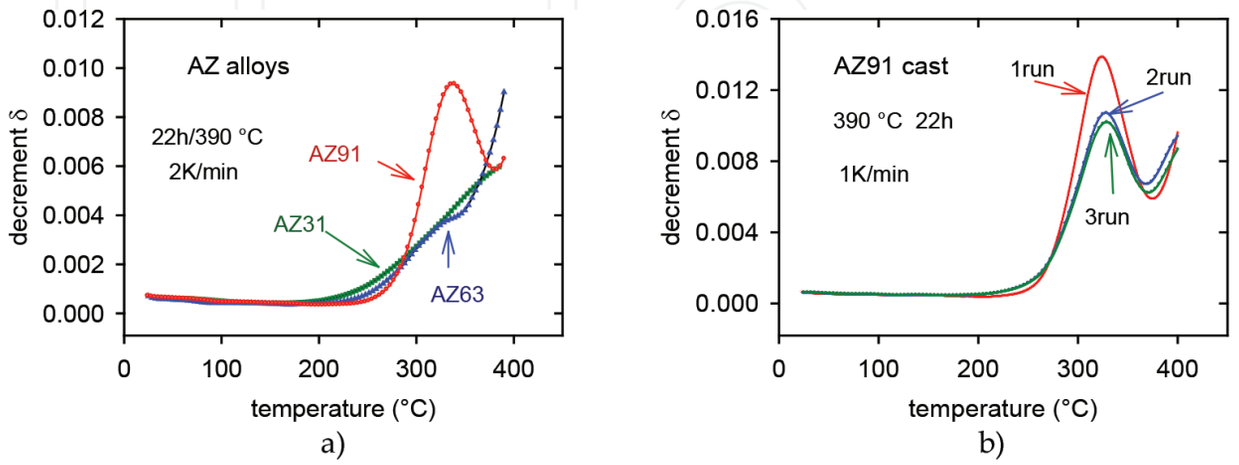

Figure 19. Temperature dependence of the decrement measured for three AZ alloys (a) and AZ91 alloy in three runs (b).

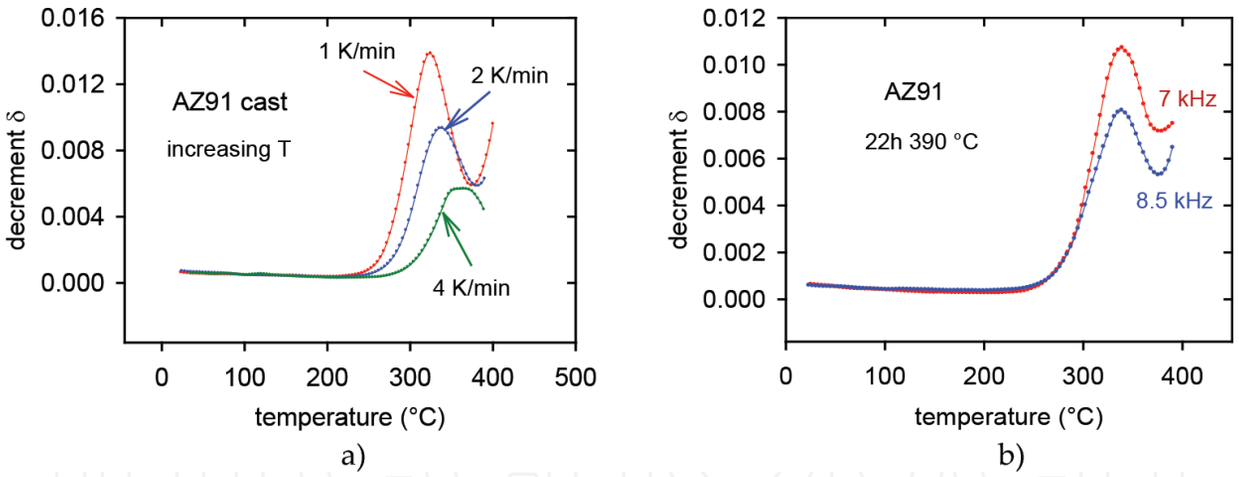

Figure 20. Temperature dependence of the logarithmic decrement while heating performed in three runs for the heating rate 1 K/min (a) and for three heating rates (b).

In the temperature dependence of the logarithmic decrement, four characteristic points were selected: 220, 320, 360 and 390°C. Samples were subjected to the homogenisation treatment and then put into a furnace with the predetermined heating rate of 1 K/min. Reaching the chosen temperature, samples were step by step removed from the furnace and quenched into water of 60°C. Scanning electron microscopy (SEM) observations were performed at room temperature. After heating of the sample with the heating rate of 1 K/min up to 220°C super-saturated solid solution decomposed; DP appeared in the vicinity of grain boundaries as it is obvious from **Figure 21a**, small precipitates visible as light points are CP, their size slowly

http://dx.doi.org/10.5772/67028

increased. Tiny CPs are situated primarily in the annealing twins, the matrix in the vicinity of twins is purified, density of CPs is in these places lower (**Figure 21b**).

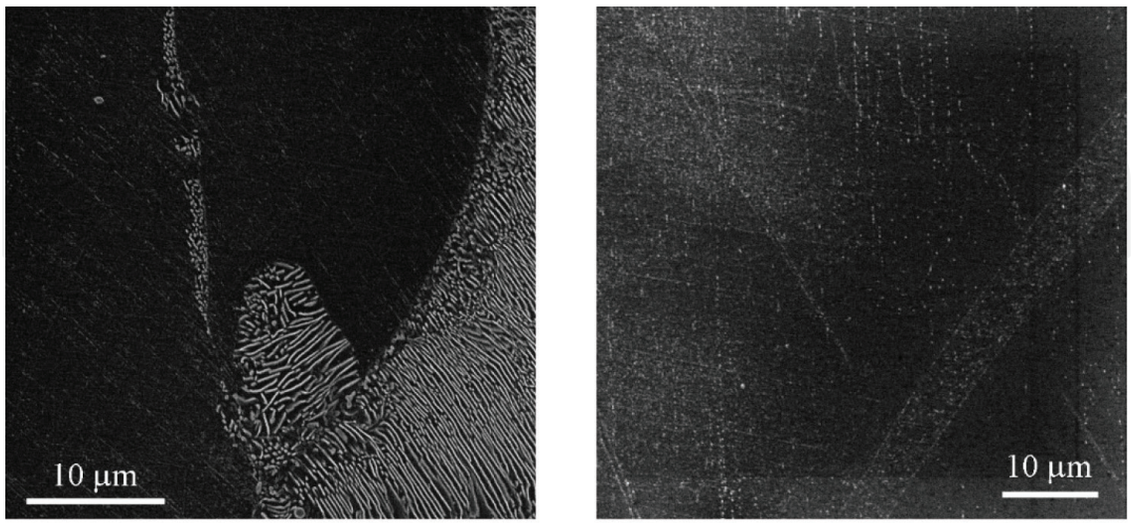

Figure 21. Microstructure of the alloy observed homogenisation and linear heating up to 220 °C: discontinuous precipitates (a), small continuous precipitates (b).

When temperature increased up to 320°C, decomposition of DPs started, and then the growing of CPs (**Figure 22a**) followed. Original lamellae were reshaped into small discs as it is visible in **Figure 22b**. CPs depicts the twin; small discs of CPs are ordered in twin/grain boundaries. Note that a temperature of 320°C corresponds to the peak temperature in the temperature dependence of decrement.

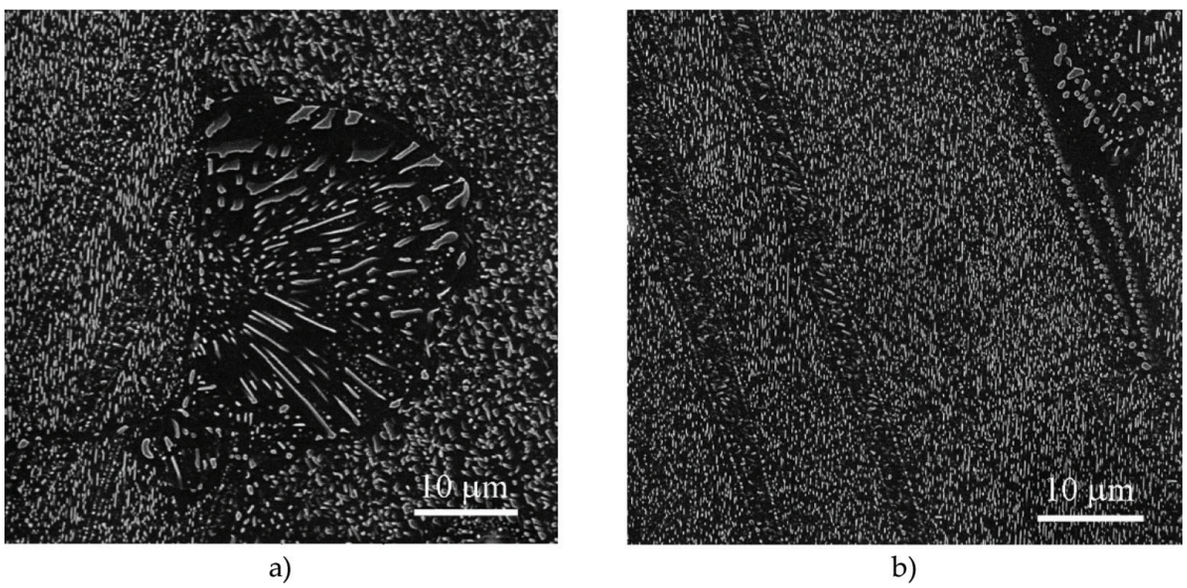

Figure 22. Microstructure of the sample subjected to homogenisation treatment and annealed up to 320 °C: decomposition of discontinuous precipitates (a), continuous precipitates situated in twins.

Microstructure of the sample annealed up to 360°C (local minimum in the temperature dependence of decrement) is characterised by the growth of CP (**Figure 23a**). Light points are small Mn particles; small content of Mn (0.24 wt.%) was used for grain refining. In the vicinity of grain boundaries, purified places were established (**Figure 23b**). Meander-like grain boundaries are decorated with larger precipitates (**Figure 23a**, **b**).

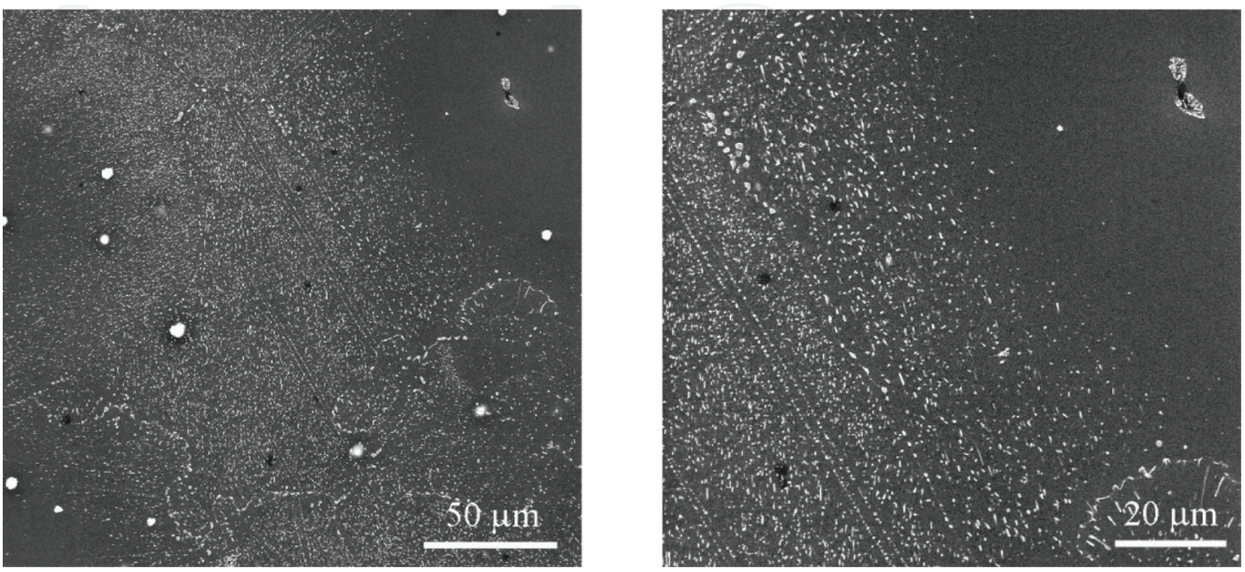

Figure 23. Microstructure of the sample after homogenisation treatment and annealed up to 360 °C: growing continuous precipitates (a), purified place free of precipitates in the upper right corner (b).

At 390°C, the transformation of DP into CP is finished. The CPs decorate the grain boundaries (**Figure 24a**), DP vanished as it is obvious from **Figure 24b** and the size of CP increased. It is possible to conclude from the microstructure observations that, in the temperature range from 220 to 360°C, a transformation of DP originally formed up to 220°C stepwise passed off. Disc-shaped CP changed into small spheres and at the highest temperatures into larger particles with a complex shape. Increasing the heating rate, time for the transformation of DP into CP is shorter. It is very probably the reason why the maximum height decreases with increasing heating rate and at the same time, the maximum is shifted to higher temperatures. DPs are formed when the grain boundary diffusion is dominant, whereas the CPs are formed at higher temperatures from solid solution when volume diffusion becomes faster. As it was shown in previous paragraphs, internal friction is very sensitive to the material microstructure, volume fraction and distribution of structural defects. Any modification in the microstructure induces changes in the internal friction course. Thus, the internal friction measurements may provide information about processes occurring at the atomic scale. Internal friction maxima were found in the AZ magnesium alloys by several authors. Lambri and co-workers [11] found the internal friction peak at about 152°C using the measuring frequency of 1 Hz. Authors ascribed this peak to the grain boundary sliding. The peak height may be controlled by a decrease in solute atoms due to precipitation process. The activation energy estimated from the Arrhenius plot was evaluated as 1.13 eV. Similarly, Liu and co-workers [55] found the internal friction peak situated at 165°C and a frequency of 1 Hz. They determined the corresponding activation energy of 1.26 eV. The peak was

ascribed to the grain boundary relaxation. Two internal friction peaks were observed in [19]. P_1 peak estimated at 165°C was characterised by the activation energy of 1.31 eV and the high temperature P_2 peak was found to be sensitive to the heating rate and insensitive to the measuring frequency. Analogous peak to the P_2 internal friction peak was estimated also by Soviarová et al. [28] at 320°C, frequency of 20.4 kHz and a heating rate of 1 K/min. Theoretical models of the internal friction consider that transformations in the solid state may be manifested by internal friction peaks. Damping mechanism can be associated with the kinetics of atoms diffusing to evolving precipitates [56]. Observed independence of the maximum position on frequency indicates that the Arrhenius equation cannot be considered in this case, that is, the interface relaxation and diffusion processes may be excluded as the reason for the maximum occurrence. During the IF measurement, the movable γ-$Mg_{17}Al_{12}$/δ-Mg interface consumes the work. When a new interface forms, defects (solute atoms and vacancies) diffuse and accumulate in the interface which leads to the gradual pinning of the interface. The movable space is a function of heating time, that is, the heating rate. The mobile interface stabilises, so that the internal friction decreases.

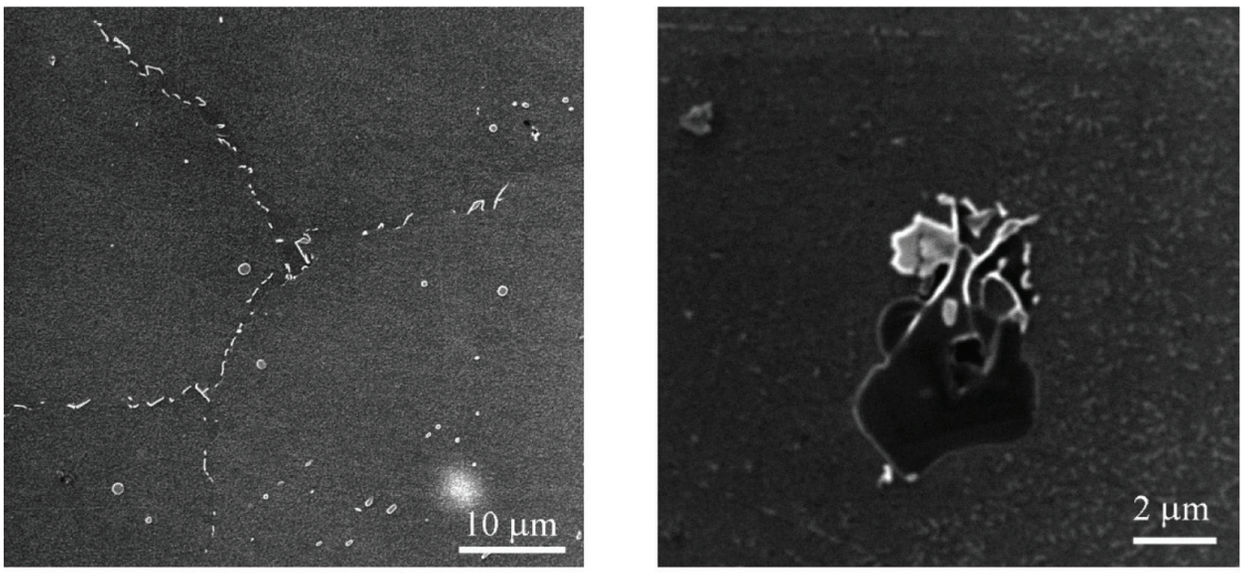

Figure 24. Microstructure of the sample after homogenisation treatment and annealed up to 390 °C: continuous precipitates in grain boundaries (a), particle of γ-$Mg_{17}Al_{12}$ phase (b).

3.3.1. Summary

Internal friction measurements of the AZ31, AZ63 and AZ91 alloys showed an exponential increase of the logarithmic decrement with temperature. In AZ63 and AZ91 alloys, this increase is modulated by a local maximum at about of 320°C. The maximum height decreased in the second and third run while the maximum temperature remained the same. The position of the local maximum was sensitive to the heating rate and insensitive to the frequency. Increasing heating rate shifted the peak temperature to higher temperatures. The occurrence of the internal friction maximum is connected with the transformation of discontinuous precipitates to continuous ones. Strain (stress)-supported flux of solute atoms and movement of

the γ-$Mg_{17}Al_{12}$/δ-Mg interface are very probably the reason for the absorption of mechanical energy carried by an ultrasonic wave.

Acknowledgements

Z.T. and P.L. gratefully acknowledge the financial support from the Czech Science Foundation under Grant 107-15/11879S. P.P. and M.C. are grateful to the Ministry of Education and Academy of Science of the Slovak Republic for the support by the project VEGA No. 1/0683/15. Parts of this chapter are reproduced from authors' recent publications [34, 41] and conference contributions [15, 36]. We thank our co-authors for permission to reuse parts of the papers. This chapter is dedicated in the memory of Professor Werner Riehemann from the Clausthal University of Technology, who passed away in January 2016.

Nomenclature

Quantities (selected)	**Materials**
σ, ε stress, strain amplitude;	AZ31 Mg-3wt%Al-1wt%Zn
δ, logarithmic decrement;	AZ63 Mg-6wt%Al-3wt%Zn
tanφ loss factor;	AZ91 Mg-9wt%Al-3wt%Zn
Q quality factor;	AM20 Mg-2wt%Al-0.4wt%Mn
ρ dislocation density	AX41 Mg-4wt%Al-1wt%Ca
ΔH activation enthalpy;	ZC63 Mg-6wt%Zn-3wt%Cu
V activation volume;	QE22 Mg-2wt%Ag-2wt%RE
λ, L_N length of dislocation segments	Saffil® 96-97%Al_2O_3, 4 to 3%SiO_2
b Burgers vector of dislocations	μMg microcrystalline Mg
τ relaxation time	UFG-Mg ultrafine-grained Mg
ω angular frequency	nGr graphite nanoparticles
α thermal expansion coefficient	nZrO_2 zirconia nanoparticles

Author details

Zuzanka Trojanová[1]*, Peter Palček[2], Pavel Lukáč[1] and Mária Chalupová[2]

*Address all correspondence to: ztrojan@met.mff.cuni.cz

1 Department of Physics of Materials, Faculty Mathematics and Physics, Charles University, Prague, Czech Republic

2 Department of Materials Engineering, Faculty of Mechanical Engineering, University of Žilina, Žilina, Slovakia

References

[1] Granato AV, Lücke K: Theory of mechanical damping due to dislocations. J. Appl. Phys. 1956; **27**:583–593. http://dx.doi.org/10.1063/1.1722436.

[2] Granato AV, Lücke K: Application of dislocation theory to internal friction phenomena at high frequencies. J. Appl. Phys. 1956; **27**:789–805. http://dx.doi.org/10.1063/1.1722485

[3] Granato AV, Lücke K: Temperature dependence of amplitude-dependent dislocation damping. J. Appl. Phys. 1981;**52**: 7136–7142. http://dx.doi.org/10.1063/1.328687

[4] Kê TS: Stress relaxation across grain boundaries in metals. Phys. Rev. 1947;**72**: 41–46.

[5] Hu XS, Zhang YK, Zheng MY, Wu K: A study of damping capacities in pure magnesium and Mg-Ni alloy. Scr. Mater. 2005;**52**:1141–1145.

[6] Hu XS, Wang XJ, He XD, Wu K, Zheng MY: Low frequency damping capacities of commercial pure magnesium. Trans. Nonferrous Met. Soc. China 2012;**22**:1907–1911. DOI: 10.1016/S1003-6326(11)61406-4

[7] Fan GD, Zheng MY, Hu XS, Xu C, Wu K, Golovin IS: Effect of heat treatment on internal friction in ECAP processed commercial pure Mg. J. Alloys Compd. 2013;**549**:38–45. doi: 10.1016/j.jallcom.2012.09.040

[8] Fan GD, Zheng MY, Hu XS, Wu K, Gan WM, Brokmeier HG: Internal friction and microplastic deformation behavior of pure magnesium processed by equal channel angular pressing. Mater. Sci. Eng A 2013; **561**:100–108. doi: 10.1016/j.msea.2012.10.083

[9] Esnouf C, Fantozzi G: Medium temperature internal friction in high purity f.c.c and h.c.p metals. J. Phys. C5, 1981;445–450. Doi: 10.1051/jphyscol:1981566

[10] Jiang WB, Kong QP, Magalas LB, Fang QF: The internal friction of single crystals, bicrystals and polycrystals of pure magnesium. Archives of Metallurgy and Materials 2015; **60**:371–375. doi:10.1515/amm-2015-0061

[11] Lambri OA, Riehemann W, Trojanová Z: Mechanical spectroscopy of commercial AZ91 magnesium alloy. Scripta Mater. 2001;**45**:1365–1371. http://dx.doi.org/10.1016/S1359-6462(01)01171-X DOI:10.1016/S1359-6462(01)01171-X#doilink

[12] Fantozzi G, Esnouf C, Benoit W, Ritchie I: Internal friction and microdeformation due to the intrinsic properties of dislocations: The Bordoni relaxations. Prog. Mater. Sci.1982;**27**:311–451. doi:10.1016/0079-6425(82)90003-2

[13] Seyed Reihani SM, Fantozzi G, Esnouf C, Revel G: Frottement intérieur d'un magnésium de haute pureté déformé plastiquement (Internal friction in high purity magnesium plastically deformed). J. Phys. Lett. 1978;**39**:L-429–432. http://dx.doi.org/10.1051/jphyslet:019780039022042900

[14] Nó ML, Oleaga A, Esnouf C, San Juan J: 1990, Internal friction at medium temperatures in high purity magnesium. Phys. Stat. Sol. (a) 1990;**120**:419–427. doi:10.1002/pssa.2211200214

[15] Trojanová Z, Weidenfeller B, Lukáč P, Riehemann W, Staněk M: Anelastic properties of nanocrystalline magnesium, in: M.J. Zehetbauer, R.Z. Valiev editors Nanomaterials by severe plastic deformation, Weiheim: Wiley VCH-Verlag GmBH; 2004. 413–419.

[16] Trojanová Z, Lukáč P, Száraz Z, Drozd Z: Mechanical and acoustic properties of magnesium alloys based (nano) composites prepared by powder metallurgical routs. In: Light Metal Alloys Applications, InTech, Rijeka 2014, 163. ISBN 980-953-307-1127-9, 163–198. http://dx.doi.org/10.5772/57454

[17] González-Martínez R, Göken J, Letzig D, Timmerberg J, Steinhoff K: Influence of heat treatment on damping behaviour of the magnesium wrought alloy AZ61. Acta Metall. Sin. 2007;**20**:235–240. doi: 10.1016/S1006-7191(07)60033-7

[18] González-Martínez R, Göken J, Letzig D, Steinhoff K, Kainer KU**:** Influence of aging on damping of the magnesium-aluminium-zinc series. J. Alloys Compd. 2007;**437**:127–132. http://dx.doi.org/10.1016/j.jallcom.2006.07.085 DOI:10.1016/j.jallcom.2006.07.085#doilink

[19] Hao GL, Han FS, Wang QZ, Wu J: Internal friction peaks associated with the precipitation in AZ91 magnesium alloy. Phys. B 2007;**391**:186–192. http://dx.doi.org/10.1016/j.physb.2006.09.018 DOI:10.1016/j.physb.2006.09.018#doilink

[20] Fan GD, Zheng MY, Hu XS, Xu C, Wu K, Golovin IS: Improved mechanical property and internal friction of pure magnesium processed by ECAP. Mater. Sci. Eng. A 2012;**566**: 588–594.http://dx.doi.org/10.1016/j.msea.2012.07.031DOI:10.1016/j.msea.2012.07.031#doilink

[21] Zhou H, Wang J-F, Pan F-S, Xu D-D, Tang A-T, Hao LH: Influence of rolling on internal friction peak of Mg3Cu1Mn alloy. Trans. Nonferrous Met. Soc. China 2013;**23**:1610–1616. doi:10.1016/S1003-6326(13)62638-2

[22] Schoeck G: Internal friction due to precipitation. Phys. Stat. Sol. (b) 1969;**32**:651–658. doi: 10.1002/pssb.19690320216

[23] Cui Y, Li Y, Sun S, Bian H, Huang H, Wang Z, Koizumi Y, Chiba A: Enhanced damping capacity of magnesium alloys by tensile twin boundaries. Scr. Mater. 2015;**101**:8–11. http://dx.doi.org/10.1016/j.scriptamat.2015.01.002

[24] Mayencourt C, Schaller R: A theoretical approach to the thermal transient mechanical loss in Mg matrix composites. Acta Mater. 1998;**46**:6103–6114. http://dx.doi.org/10.1016/S1359-6454(98)00274-2

[25] Carreño-Morelli E, Urreta SE, Schaller R: Mechanical spectroscopy of thermal stress relaxation at metal-ceramic interfaces in aluminium-based composites. Acta Mater. 2000;**48**:4725–4733. http://dx.doi.org/10.1016/S1359-6454(00)00264-0

[26] Trojanová Z, Weidenfeller B, Riehemann W: Thermal stresses in a Mg-Ag-Nd alloy reinforced by short Saffil fibres studied by internal friction. Mater. Sci. Eng. A 2006;**442**:480–483. http://dx.doi.org/10.1016/j.msea.2006.04.137

[27] Lukáč P, Trojanová Z: Hardening and softening in selected Mg alloys, Mater. Sci. Eng. A 2007;**462**:23–28. http://dx.doi.org/10.1016/j.msea.2006.01.170

[28] Soviarová A, Palček P, Trojanová Z: 2014, Monitoring of precipitation process in AZ31 and AZ91 magnesium alloys by internal damping measurement, Manuf. Technol. 2014;**14**:447–451.

[29] D'Anna G, Benoit W, Vinokur VM: Internal friction and dislocation collective pinning in disordered quenched solid solutions. J. Appl. Phys. 1997;**82**:5983–5990. http://dx.doi.org/10.1063/1.366463

[30] Farkas G, Trojanová Z, Száraz Z, Minárik P, Máthis K: Effect of the fiber orientation on the deformation mechanisms of magnesium-alloy based fiber reinforced composite. Mater. Sci. Eng. A, 2015;**643**:25–31. 10.1016/j.msea.2015.07.012

[31] Chmelík F, Kiehn J, Lukáč P, Kainer K-U, Mordike BL: Acoustic emission and dilatometry for non-destructive characterisation of microstructural changes in Mg based metal matrix composites submitted to thermal cycling. Scripta Mater. 1998;**38**:81–88. 10.1016/S1359-6462(97)00416-8

[32] Kiehn J, Z. Trojanová Z, Lukáč P, K. U. Kainer KU: Effect of thermal cycling on the damping behaviour of Mg matrix composites. Key Eng. Mat. 1997;**127–131**:993–1000. 195.113.32.106-03/05/07,11:38:39)

[33] Chmelík F, Trojanová Z, Kiehn J, Lukáč P, Kainer KU: Non-destructive characterisation of microstructure evolution in Mg based metal matrix composites submitted to thermal cycling. Mater. Sci. Eng. 1997;A**234**–**236**:774–777. PII S0921-5093(97)00401-2

[34] Z. Trojanová, P. Lukáč: Microstructure changes in magnesium alloys base composites studied by internal friction. Acta Univ. Carol. Math. Phys. 2005;**46:**11–25.

[35] Carreño-Morelli E, Urreta SE, Schaller R, In: Proceedings of the International Conference on Fatigue of Composites (S. Degallaix, C. Bathias, R. Fougères, eds.), Société Française de Métallurgie et de Matériaux, Paris, 1997,France, 112–119.

[36] Riehemann W, Trojanová Z, Mielczarek A: Fatigue in magnesium alloy AZ91-gamma Alumina fiber composite studied by internal friction measurements FATIGUE 2010. Proc. Eng. 2010;**2**:2151–2160. 10.1016/j.proeng.2010.03.231

[37] Lemaitre J: A Course on Damage Mechanics. Berlin 1996, Springer. ISBN 978-3-642-18255-6

[38] Göken J, Riehemann W: Damping behaviour of AZ91 magnesium alloy with cracks. Mater. Sci. Eng. A 2004;**370**:417–421. doi:10.1016/j.msea.2003.08.110

[39] Nowick AS, Berry BS: Anelastic relaxations in crystalline solids. Academic Press, 1972; New York, NY/London.

[40] Trojanová Z, Lukáč P, Weidenfeller B, Riehemann W: Mechanical damping in magnesium prepared by ball milling in medium temperature region. Kovove Mater. 2008;**46:**249–256.

[41] Trojanová Z, Lukáč P: Elastic and plastic properties of ultra-fine grained magnesium. Int. J. Mater. Product Technol. 2011;**40**:120–139. doi: 10.1504/IJMPT.2011.037209

[42] Seyed Reihani SM, Fantozzi G, Esnouf C, Revel G: 1979, Internal friction of high purity magnesium after plastic deformation. Scripta Metall. 1979;**13**:1011–1015. doi:10.1016/0036-9748(79)90194-7

[43] Fantozzi G, Esnouf C, Seyed Reihani SM, Revel G: 1984, Anelastic behaviour of plastically deformed high purity magnesium between 10 and 500 K. Acta Metall. 1984;**32**:2175–2183. doi:10.1016/0001-6160(84)90160-3

[44] Nó ML. Dislocation damping at medium temperature. In: Schaller R, Fantozzi G, Gremaud G, editors. Mechanical Spectroscopy Q^{-1} 2001. Trans Tech Publications Ltd 2001, Switzerland, 247–267.

[45] Trojanová Z, Bosse M, Ziegmann G, Mielczarek A, Ferkel H: Anelastic properties of Mg+3vol.%Gr prepared by ball milling. Key Eng. Mater. 2006;**319**:189–195. 195.113.32. 106-03/05/07,11:37:04

[46] Couret A, Caillard D: An in situ study of prismatic glide in magnesium—I. The rate controlling mechanism. Acta Metall. 1985;**33**: 1447–1454. doi:10.1016/0001-6160(85)90045-8

[47] Courret A, Caillard D: An *in situ* study of prismatic glide in magnesium—II. Microscopic activation parameters, Acta Metall. 1985;**33**:1455–1462. doi:10.1016/0001-6160(85)90046-X

[48] Lakki A, Schaller R, Carry C, Benoit W: High temperature anelastic and viscoplastic deformation of fine-grained MgO-doped Al_2O_3. Acta Mater. 1998;**46**:689–700. http://dx.doi.org/10.1016/S1359-6454(97)00250-4

[49] Frost JH, Ashby MF: Deformation Mechanisms Maps. Pergamon Press; 1982, Oxford.

[50] Arsenault RJ, Shi N: Dislocation generation due to differences between the coefficients of thermal expansion. Mater. Sci. Eng. 1986;**81**:175–187. doi:10.1016/0025-5416(86)90261-2

[51] Rawal SP: Interface structure in graphite-fiber-reinforced metal–matrix composites. Surf. Interface Anal. 2001;**31**:692–700.

[52] Ibrahim IA, Mohamed FA, Lavernia EJ: Particulate reinforced metal matrix composites—a review. J. Mater. Sci. 1991;**26**:1137–1156. doi: 10.1007/BF00544448

[53] Vincent A, Lormand S, Durieux S, Girard C, Maire E, Fougères R: Transient internal damping in metal matrix composites: Exp. Theory. J. Phys. IV 1996;**6**:C8:719–730.doi: 10.1051/jp4:19968157

[54] Wei LN, Li ZB, Han, F.S. 2002, Thermal mismatch dislocations in macroscopic graphite particle-reinforced metal matrix composites studied by internal friction. Phys. Stat. Sol. (a) 2002;**191**:125–136. doi: 10.1002/1521-396X(200205)191:1<125::AID-PSSA125>3.0.CO;2-2

[55] Liu S-W. Jiang H-C, Li X-Y, Rong L-J: Effect of precipitation on internal friction of AZ91 magnesium alloy. Trans. Nonferrous Met. Soc. China 2010;**20**:453–457. doi:10.1016/S1003-6326(10)60517-1

[56] Song Z, Kishimoto S, Zhu J, Wang Y: Study of stabilization of CuAlBe alloy during martensitic transformation by internal friction. Solid State Commun. 2006;**139**:235–239. http://dx.doi.org/10.1016/j.ssc.2006.05.037